JGR Space Physics

RESEARCH ARTICLE
10.1029/2021JA029863

Ion Dynamics at the Magnetopause of Ganymede

S. Fatemi[1], A. R. Poppe[2], A. Vorburger[1,3], J. Lindkvist[1], and M. Hamrin[1]

[1]Department of Physics, Umeå University, Umeå, Sweden, [2]Space Sciences Laboratory, University of California at Berkeley, Berkeley, CA, USA, [3]Physics Institute, University of Bern, Bern, Switzerland

Key Points:

- The Hall electric field dominates at the magnetopause and in the magnetotail of Ganymede, accelerating Jovian magnetospheric ions
- Magnetopause interaction increases the energy of O^+ and H^+ ions by a factor of 8 and 30, respectively
- The incident Jovian plasma upstream of Ganymede's magnetopause is highly non-Maxwellian and accelerated up to 1 MeV at the magnetopause

Correspondence to:
S. Fatemi,
shahab.fatemi@umu.se

Citation:
Fatemi, S., Poppe, A. R., Vorburger, A., Lindkvist, J., & Hamrin, M. (2022). Ion dynamics at the magnetopause of Ganymede. *Journal of Geophysical Research: Space Physics*, *127*, e2021JA029863. https://doi.org/10.1029/2021JA029863

Received 10 AUG 2021
Accepted 4 JAN 2022

Abstract We study the dynamics of the thermal O^+ and H^+ ions at Ganymede's magnetopause when Ganymede is inside and outside of the Jovian plasma sheet using a three-dimensional hybrid model of plasma (kinetic ions, fluid electrons). We present the global structure of the electric fields and power density ($\mathbf{E} \cdot \mathbf{J}$) in the magnetosphere of Ganymede and show that the power density at the magnetopause is mainly positive and on average is +0.95 and +0.75 nW/m^3 when Ganymede is inside and outside the Jovian plasma sheet, respectively, but locally it reaches over +20 nW/m^3. Our kinetic simulations show that ion velocity distributions at the vicinity of the upstream magnetopause of Ganymede are highly non-Maxwellian. We investigate the energization of the ions interacting with the magnetopause and find that the energy of those particles on average increases by a factor of 8 and 30 for the O^+ and H^+ ions, respectively. The energy of these ions is mostly within 1–100 keV for both species after interaction with the magnetopause, but a few percentages reach to 0.1–1 MeV. Our kinetic simulations show that a small fraction (<25%) of the corotating Jovian plasma reach the magnetopause, but among those >50% cross the high-power density regions at the magnetopause and gain energy. Finally, we compare our simulation results with Galileo observations of Ganymede's magnetopause crossings (i.e., G8 and G28 flybys). There is an excellent agreement between our simulations and observations, particularly our simulations fully capture the size and structure of the magnetosphere.

1. Introduction

Ganymede, the largest Galilean moon of Jupiter and the largest moon of our solar system (Ganymede's radius $R_G \approx 2{,}630$ km), is the only known moon today that possesses a global, intrinsic magnetic field of internal origin (Gurnett et al., 1996; Kivelson et al., 1996, 2002). Ganymede's equatorial surface field strength is ~719 nT, which is nearly an order of magnitude stronger than the ambient Jovian magnetic field at Ganymede's orbital distance (Kivelson et al., 1996, 2002). This field is strong enough to stand-off the incident Jovian magnetospheric plasma at ~1R_G upstream of Ganymede's surface and carves out a small magnetosphere within the larger magnetosphere of Jupiter (e.g., Gurnett et al., 1996; Jia et al., 2008; Kivelson et al., 1996, 1997, 2002; Volwerk et al., 1999).

At Ganymede's orbit ~15 Jupiter's radii, the Jovian magnetospheric plasma, which nearly corotates with Jupiter (Frank et al., 1976; Krimigis et al., 1979), moves faster than the Keplerian speed of Ganymede. Therefore, the plasma overtakes the orbital trailing hemisphere of Ganymede at a relative speed of ~140 km/s (e.g., Kivelson et al., 2004; Williams et al., 1997). Due to the ~10° tilt of Jupiter's magnetic moment from its rotation axis (e.g., Acuna & Ness, 1976), Ganymede experiences different plasma and magnetic field environments that vary slowly with ~10.5-hr period of Jupiter's synodic rotation (e.g., Kivelson et al., 1997, 1998).

When Ganymede is inside the Jovian plasma sheet, the plasma density is higher and the magnetic field intensity is slightly lower than those outside the plasma sheet. Plasma β (the ratio between plasma thermal pressure and magnetic pressure) inside the plasma sheet is slightly larger than unity whereas it is below one outside the plasma sheet (e.g., Jia et al., 2009a; Kivelson et al., 2004). The sonic and Alfvenic Mach numbers, however, are smaller than one in both of these regions (e.g., Jia et al., 2008, 2009a; Kivelson et al., 2004; Neubauer, 1998). In this interaction regime, unlike planetary magnetospheres, no bow shock forms (e.g., Kivelson et al., 2004; Neubauer, 1998; Volwerk et al., 1999). Instead, compressional waves propagate upstream that decelerate the incident plasma and divert the plasma flow around the magnetosphere, resulting in bending of the magnetic field lines and the formation of the Alfvén wings (Kivelson et al., 2002, 2004; Neubauer, 1998). Therefore, it is expected that the Jovian plasma directly interacts with the magnetosphere of Ganymede without being significantly distorted.

The magnetosphere of Ganymede consists of closed and open magnetic field line regions (e.g., Kivelson et al., 1996; Volwerk et al., 1999; Williams et al., 1998). The closed field line region covers the low latitudes near

the equator, forms a magnetopause close to Ganymede at $\sim 1R_G$ above the surface (e.g., Jia et al., 2008, 2010; Kivelson et al., 1996, 1997; Kopp & Ip, 2002; Paty & Winglee, 2004; Williams et al., 1998), and limits the access of plasma to low latitudes on the trailing hemisphere of Ganymede (e.g., Cooper et al., 2001; Fatemi et al., 2016; Liuzzo et al., 2020; Plainaki et al., 2020, 2015; Poppe et al., 2018; Volwerk et al., 1999). On the contrary, the open magnetic field line region covers a relatively large area over the poles that enables the access of plasma to the surface (e.g., Cooper et al., 2001; Fatemi et al., 2016; Liuzzo et al., 2020; Plainaki et al., 2020, 2015; Poppe et al., 2018) and connects the magnetosphere of Ganymede to Jupiter (Kivelson et al., 1996, 2002; Neubauer, 1998).

With a highly efficient magnetic reconnection rate at Ganymede's magnetopause (e.g., Collinson et al., 2018; Jia et al., 2010; Kivelson et al., 1998; Tóth et al., 2016; Volwerk et al., 1999; Zhou et al., 2020), Ganymede's magnetosphere is considered as a favorable magnetic reconnection laboratory. This is mainly because (a) the Jovian magnetic fields always remain in opposite directions to the equatorial fields of Ganymede, and are thus, favorably oriented for reconnection (e.g., Jia et al., 2009a, 2010; Kivelson et al., 2004), (b) the Jovian magnetospheric conditions are relatively stable upstream of Ganymede as opposed to the highly variable solar wind upstream of planetary magnetospheres (e.g., Jia et al., 2009a; Kivelson et al., 2004), and (c) plasma β is often smaller than one, as Ganymede is mainly outside the Jovian plasma sheet (e.g., Jia et al., 2009a; Kivelson et al., 2004). A combination of low plasma β and large magnetic shear angle provides a high reconnection rate (e.g., Paschmann et al., 2013; Phan et al., 2010).

Magnetic reconnection is believed to control the energy input into the planetary magnetospheres from the incident plasma and hence the rate of convection in the magnetospheres (e.g., Dungey, 1961; Russell, 2000). The steady and slowly varying magnetic field of Jupiter was expected to drive a steady, and not a bursty reconnection at Ganymede (Jia et al., 2009a; Kivelson et al., 2004). However, MHD simulations have suggested that magnetic reconnection at Ganymede is predominantly intermittent, leading to the formation of flux transfer events at the magnetopause (Jia et al., 2010; Tóth et al., 2016; Zhou et al., 2020). These processes may deplete the closed field lines from plasma at close distances ($<1R_G$) to Ganymede (Volwerk et al., 1999; Williams et al., 1998). Moreover, Galileo observations inside Ganymede's polar cap indicated a high reconnection efficiency at the magnetopause (Collinson et al., 2018; Kivelson et al., 1997), as well as reconnection-driven plasma flows at low-latitude magnetospheric boundaries (Collinson et al., 2018). When Ganymede is inside the Jovian plasma sheet, recent MHD simulations combined with kinetic particle models (MHD-EPIC) have estimated that the global reconnection rate at Ganymede is ~80 kV with 60% efficiency (Zhou et al., 2020), which is lower that an upper limit of 100% reconnection efficiency suggested by Kivelson et al. (1997) when Ganymede is outside the plasma sheet.

Here, we use a three-dimensional hybrid-kinetic model of plasma to investigate ion dynamics at Ganymede's magnetopause. We examine the contribution of the electric field in particle energization and identify regions for particle acceleration and deceleration. We also estimate how much the magnetospheric plasma can be accelerated due to the interaction with Ganymede's magnetopause and calculate the rate of particles that cross the upstream magnetopause and gain energy. These analyses are important to better understand the plasma environment of Ganymede and future plasma observations in Ganymede's magnetosphere by ESA's JUpiter ICy moons Explorer (JUICE) mission (Grasset et al., 2013), where Ganymede is the primary scientific target of the mission.

2. Model and Methodology

2.1. Multi-GPU-Based Hybrid Model of Plasma

We use an upgraded version of the Amitis code (Fatemi et al., 2017) that runs on multiple Graphics Processing Units (GPUs) instead of a single GPU. Amitis is a three-dimensional grid-based hybrid model of plasma (ions are macroparticles and electrons are a mass-less charge-neutralizing fluid) that runs at least 10 times faster and is more energy and cost efficient compared to its parallel CPU-based predecessors (Fatemi et al., 2017).

In our model, an ion position, $\mathbf{r}_i$, and velocity, $\mathbf{v}_i$, are obtained from the Lorentz equation of motion

$$\frac{d\mathbf{v}_i}{dt} = \frac{q_i}{m_i}\left(\mathbf{E} + \mathbf{v}_i \times \mathbf{B}\right), \quad \frac{d\mathbf{r}_i}{dt} = \mathbf{v}_i, \tag{1}$$

where q_i and m_i are, respectively, the charge and mass of a macroparticle ion, $\mathbf{E}$ is the electric field, and $\mathbf{B}$ is the magnetic field applied to the ion at its position. We calculate the electric field from the electron momentum equation for mass-less electrons ($m_e = 0$), which is given by

$$\mathbf{E} = \overbrace{-\mathbf{u}_i \times \mathbf{B}}^{\text{Convective}} + \overbrace{\mathbf{J} \times \mathbf{B}/\rho_i}^{\text{Hall}} + \overbrace{\eta \mathbf{J}}^{\text{Ohmic}} - \overbrace{\nabla P_e/\rho_i}^{\text{Ambipolar}}, \tag{2}$$

where $\mathbf{u}_i$ and ρ_i are the bulk flow velocity and charge density of macroparticle ions, respectively, $\mathbf{J}$ is the total current density obtained from Ampere's law (i.e., $\mathbf{J} = \nabla \times \mathbf{B}/\mu_0$), η is the resistivity, and P_e is the electron pressure. For the presented results in this study, we assumed that electrons are an ideal gas and P_e is adiabatic with index $\gamma = 1.667$. Different electric field terms including the convective (motional), Hall, ohmic, and ambipolar are marked in Equation 2. The magnetic field is advanced in time using Faraday's law, $\partial \mathbf{B}/\partial t = -\nabla \times \mathbf{E}$. The model principles are described in detail in Fatemi et al. (2017).

To present our simulation results, we use a Ganymede-centered Cartesian coordinate system, known as "GphiO" (e.g., Jia et al., 2008; Paty & Winglee, 2004). In this system, Ganymede is located at the center of the coordinate system, the Jovian corotational plasma flows along the $+x$ axis, the $+y$ axis is along the Ganymede-Jupiter vector and points toward Jupiter, and the $+z$ axis completes the right-handed coordinate system. We assume Ganymede's surface is a perfect plasma absorber, and when a particle impacts the surface of Ganymede, it is removed from the simulation domain. We also assume that Ganymede is a nonconductive body with a uniform resistivity of 10^7 Ω m and has an internal magnetic dipole with a magnetic moment $M = 1.3 \times 10^{20}$ A m^2 located at the center of Ganymede, which provides a surface equatorial magnetic field magnitude of ∼715 nT, which is consistent with Galileo observations (Kivelson et al., 1997, 2002). In our model, plasma resistivity is 3×10^3 Ω m and to handle the vacuum regions formed in our simulations we use a vacuum resistivity of 0.3×10^7 Ω m, as explained by Fatemi et al. (2017). The vacuum resistivity is dynamically assigned to the grid cells whenever their density goes below 0.1% of the undisturbed (upstream) Jovian plasma density where we solve the magnetic diffusion equation instead of the general Faraday's law (see Fatemi et al., 2017 for details).

We perform two hybrid simulation runs for the conditions that Ganymede is inside and outside the Jovian plasma sheet. For each of these conditions, we use the plasma parameters obtained during the G8 and G28 Galileo flybys, summarized in Kivelson et al. (2004), Jia et al. (2008), and Bagenal et al. (2016). During the G8 flyby, Ganymede was inside (or close to) the Jovian plasma sheet, and during the G28 flyby, Ganymede was located outside the plasma sheet (Jia et al., 2008; Kivelson et al., 2004). For both of our simulations, we use two ion species, i.e., H^+ and O^+, that move with a bulk velocity $\mathbf{u}_0 = +140\hat{x}$ km/s in Ganymede's rest frame. We assume a mass fraction of ∼13% for H^+ and ∼87% for O^+, equivalent to a mean ion mass of 14 amu estimated from Galileo observations (Kivelson et al., 2004). In our model, H^+ temperature is 65 eV, O^+ temperature is 220 eV, and electron temperature is 100 eV, which are consistent with previous observations at Ganymede's orbit (Bagenal & Delamere, 2011; Bagenal et al., 2016; Kivelson et al., 2004). It is possible that S^{++} ions also contribute in a considerable fraction of the thermal plasma near the orbit of Ganymede. However, since the S^{++} and O^+ have a similar mass-to-charge ratio, we still do not know how large the contribution of S^{++} ions are from the previous observations, and thus, not included in our simulations for simplicity.

In our simulations, we only include the thermal component of the corotating ions and do not account for energetic particles. The energetic particles significantly contribute to the total pressure of plasma in MHD models (e.g., Dorelli et al., 2015; Jia et al., 2008; Tóth et al., 2016; Zhou et al., 2019). Including energetic ions in a kinetic model requires taking extremely small time steps, which would be computationally expensive even for a GPU-based model, or requires multitime stepping (e.g., Omelchenko & Karimabadi, 2006) which is not implemented in the current version of our model. Previously, Fatemi et al. (2016) accounted for energetic particles in their hybrid model by choosing a higher temperature than the average thermal plasma temperature. Although there is a fair agreement between their simulations and Galileo magnetic field observations for most of the flybys, their simulation results, similar to a few of the previous MHD simulations (e.g., Dorelli et al., 2015; Jia et al., 2008; Tóth et al., 2016), could not correctly estimate the size and structure of Ganymede's magnetopause during the G8 flyby. Here, we take a different approach and in order to account for higher pressure in our simulations, we assume the total plasma density is 8 cm^{-3} when Ganymede is inside and 6 cm^{-3} when Ganymede is outside the Jovian plasma sheet. These values are nearly 1.5–2 times higher than the average densities applied in previous simulations (e.g., Dorelli et al., 2015; Fatemi et al., 2016; Jia et al., 2008; Zhou et al., 2019). However, they are

within the observed range for thermal ions (1–10 cm^{-3}) at the orbital distance of Ganymede from Jupiter (Belcher, 1983; Kivelson et al., 2004). In addition, the applied densities and temperatures in our simulations result in the total pressure (thermal + dynamic) ∼3.8 nPa and ∼2.9 nPa during the G8 and G28 flybys, respectively, which are consistent with the applied pressure in previous MHD simulations (e.g., Dorelli et al., 2015; Duling et al., 2014; Jia et al., 2008, 2010; Tóth et al., 2016; Zhou et al., 2019).

Besides the differences in plasma environment inside and outside of the Jovian plasma sheet, a major difference between these two environments is the background Jovian magnetic field strength and orientation. We use $\mathbf{B} = (-10.0, -6.0, -86.0)$ nT when Ganymede is inside and $\mathbf{B} = (0.0, +77.0, -76.0)$ nT when Ganymede is outside the plasma sheet, which are consistent with Galileo observations (Kivelson et al., 2004) and previous MHD simulations of Ganymede (e.g., Duling et al., 2014; Zhou et al., 2019, 2020). The upstream Alfvén speed, v_A, in our simulations for the G8 and G28 flybys is ∼179 and ∼258 km/s, which leads to Alfvén Mach number, $|\mathbf{u}_0|/v_A$, 0.78 and 0.54, respectively, and thus the plasma flow is sub-Alfvénic in both environments.

We use a simulation domain of size $-8R_G \le x \le +5R_G$, $-11R_G \le y \le +11R_G$, and $-16R_G \le z \le +16R_G$ with a regular-spaced cubic cell size $\Delta L = 175$ km ($\Delta L \approx 0.06R_G$ and ≈0.4 of the ion inertial length in the Jovian plasma sheet). Our simulation time step $\Delta t = 1$ ms, which is $\sim 8 \times 10^{-5}$ of the oxygen gyroperiod and $\sim 10^{-3}$ of the proton gyroperiod in the upstream corotating plasma. Over Ganymede's poles, where the magnetic field is the strongest (≈1,440 nT on the surface), our simulation time step is equivalent to $\sim 10^{-3}$ of the O^+ gyroperiod and $\sim 2 \times 10^{-2}$ of the H^+ gyroperiod, which is small enough to fully resolve the gyromotion of the particles within the entire simulation domain. We run our simulations for 700 s, but the overall structure of Ganymede's magnetosphere reaches to a steady state after ∼250 s.

2.2. Particle Selection for Interaction With the Magnetopause

In order to provide detailed understanding on the dynamics of the corotating thermal plasma and particle interaction with Ganymede's magnetopause, we collect particles positions and velocities that interact with the upstream magnetopause. Since Ganymede's magnetosphere is dynamic and the magnetic reconnection at the magnetopause is suggested to be intermittent (Collinson et al., 2018; Jia et al., 2010; Tóth et al., 2016; Zhou et al., 2020), no steady state solution exists for Ganymede. Therefore, a test-particle approach that follows particle trajectories in a time snapshot of the electric and magnetic fields can only represent particles distribution at a given time and does not include the overall particle interaction with the dynamic magnetosphere of Ganymede, and thus, should be avoided (also see Fatemi et al., 2020 for a similar approach in the dynamic magnetosphere of Mercury).

Therefore, in this study, after the magnetosphere of Ganymede is fully developed (i.e., ∼250 s in our simulations), for every $50\Delta t$ (i.e., 50 ms) within a period of 450 s (i.e., from 250 to 700 s that we stop our simulations) we select all particles that interact with the upstream magnetopause of Ganymede. Our selection criteria for interaction with the magnetopause contains passing a particle through an electric current density larger than 0.2 $\mu A/m^2$ upstream of Ganymede. As shown later in Figure 1, the magnetopause forms at distances below $2R_G$ upstream and the y-component of the current density, which is the dominant magnetopause current during the G8 flyby, exceeds over 0.6 $\mu A/m^2$. Since the average current density upstream of Ganymede's magnetosphere and away from the magnetospheric perturbations is below 0.02 $\mu A/m^2$ in our simulations (see Figures 1f and 1g), selection of electric current density above 0.2 $\mu A/m^2$ is a valid criteria for indication of the upstream magnetopause crossing.

Most of the energy from the Jovian plasma is expected to be transferred to Ganymede's magnetosphere through magnetopause reconnection (e.g., Jia et al., 2010; Kivelson et al., 1998; Tóth et al., 2016; Zhou et al., 2020). The energy transfer at terrestrial magnetospheres and cometary atmospheres has been studied by considering the power density, $P = \mathbf{E} \cdot \mathbf{J}$, where $\mathbf{E}$ is the electric field and $\mathbf{J}$ is the electric current density (e.g., Hamrin et al., 2015, 2011; Lindkvist et al., 2018; Rosenqvist et al., 2008). In other words, the power density can be used as a primary indicator of potential reconnection sites. In the rest frame of Ganymede, if a particle passes a region with a positive power density (i.e., $\mathbf{E} \cdot \mathbf{J} > 0$, also called a "load" region), the particle gains energy, but if it passes a region with a negative power density ($\mathbf{E} \cdot \mathbf{J} < 0$, also called a "generator" region), it loses its energy and stores it into the electromagnetic energy (e.g., Hamrin et al., 2011; Lindkvist et al., 2018).

As we solve the equation of motion (Equation 1), if a particle interacts with Ganymede's magnetopause, we store its "*initial*" and "*final*" positions and velocities, as well as its position and velocity at the "*magnetopause*." The

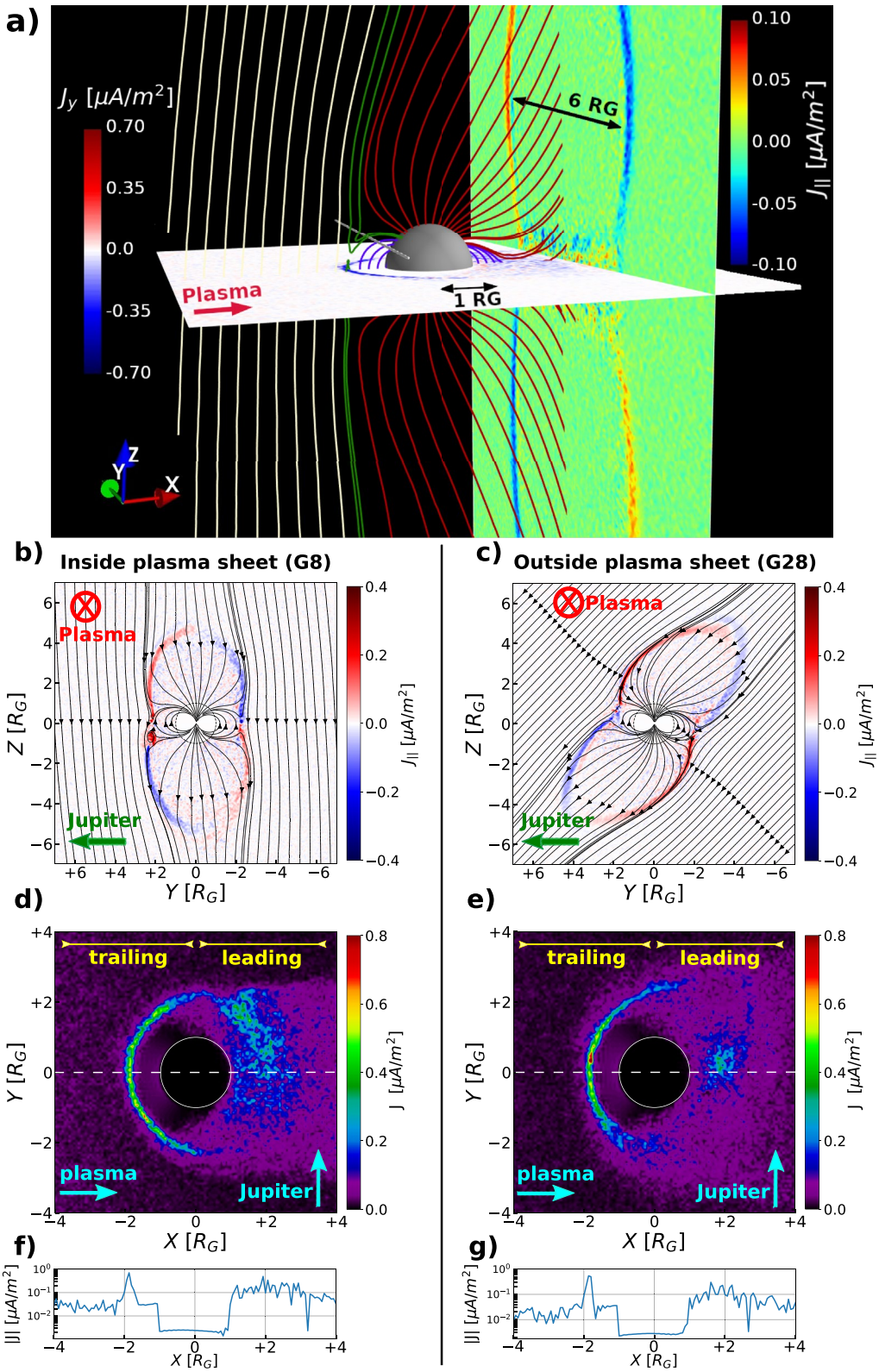
a)
J_y [$\mu A/m^2$]
0.70
0.35
0.0
-0.35
-0.70
6 RG
1 RG
Plasma
0.10
0.05
0.00
-0.05
-0.10
$J_{||}$ [$\mu A/m^2$]
Z
Y
X
b) Inside plasma sheet (G8)
c) Outside plasma sheet (G28)
Plasma
Jupiter
Z [R_G]
Y [R_G]
$J_{||}$ [$\mu A/m^2$]
d)
e)
trailing
leading
plasma
Jupiter
X [R_G]
J [$\mu A/m^2$]
f)
g)
|J| [$\mu A/m^2$]

Figure 1.

initial denotes particle's position and velocity at the inflow boundary of our simulation (i.e., $x \approx -8R_G$), and the *final* indicates particle's position and velocity when it leaves the simulation domain by either impacting on the surface of Ganymede or moving through the outflow boundary (i.e., $x \approx +5R_G$). In addition, we also mark particles that experience a positive power density larger than $P_0 = \omega_0 \rho_{m_0} u_0^2$ during the magnetopause crossing, where ω_0 is the mean ion cyclotron frequency, ρ_{m_0} is the mean mass density, and u_0 is the plasma bulk flow speed. This indicates that a region with power density of P_0 or larger has enough power to divert plasma within the time frame of a gyration period. P_0 for the G8 and G28 flybys is ~2.2 and ~2.0 nW/m^3, respectively.

To further investigate changes in the energy of the interacting ions with Ganymede's magnetopause, we calculate three types of energies for each ion: (a) the total energy, $m_i v_i^2/2$, (b) the thermal energy, $m_i v_{th}^2/2$, and (c) the parallel energy, $m_i v_\parallel^2/2$, where $v_i = |\mathbf{v}_i|^2$ is the ion speed. The thermal speed, $v_{th} = |\mathbf{v}_i - (\mathbf{B}(\mathbf{v}_i \cdot \mathbf{B}) + \mathbf{E} \times \mathbf{B}) / B^2|$, is the speed perpendicular to the magnetic field seen in the frame moving with the (momentary) $\mathbf{E} \cdot \mathbf{B}$ drift velocity. This allows the thermal energy to be larger than the total energy. The parallel speed, $v_\parallel = \mathbf{v}_i \cdot \mathbf{B}/B$, is the particle speed along the magnetic field lines, $\mathbf{B}$.

3. Results

Here, we present our hybrid simulation results for the Jovian plasma interaction with Ganymede's magnetosphere when Ganymede is inside and outside the Jovian plasma sheet. First, we show the global structure of Ganymede's magnetosphere, then we compare our simulation results with Galileo observations, and present particle interaction with the magnetopause of Ganymede. Finally, we show a few sample trajectories of the ions that interact with the magnetopause.

3.1. Structure of Ganymede's Magnetosphere

Figure 1a shows a snapshot of our hybrid simulation results when Ganymede is inside the Jovian plasma sheet (i.e., for the G8 flyby plasma conditions). It shows the y-component of the current density, J_y, in the equatorial (xy) plane at $z = 0$, and the field-aligned current density, $J_\parallel$, in the yz plane at $x \approx +3.5R_G$. We also show a few magnetic field lines in the xz plane. We have shown few samples of the closed magnetic field lines (blue) at low latitudes and open magnetic field lines (red) at high latitudes over the polar caps. We see that the open field lines over Ganymede's polar caps bend with respect to the background Jovian magnetic field, forming the Alfvén wings. The recently reconnected field lines (green) at the time snapshot of the chosen simulation results can be also seen at the boundaries between the open and closed field lines. The undisturbed Jovian magnetic fields (white) are shown upstream of Ganymede. We have also shown the Galileo's trajectory during the G8 flyby upstream of Ganymede, passing close to the boundary of the open-closed magnetic field lines.

Figures 1b and 1c show the structure of Ganymede's magnetosphere (black magnetic field lines) and the field-aligned currents (background color) in the yz plane at $x = 0$ during the G8 and G28 flybys, respectively. In these figures, the red (blue) color indicates current flow parallel (anti-parallel) to the magnetic field lines. These currents and their associated perturbations bend the magnetic field lines (red and green lines in Figure 1a) and contribute to the formation of the Alfvén wings. Consistent with previous simulations (e.g., Dorelli et al., 2015; Fatemi et al., 2016; Jia et al., 2008, 2010), the width of Ganymede's magnetosphere at $x = 0$ is ~$4R_G$ (Figure 1b), and expands to ~$6R_G$ downstream (Figure 1a). In contrast to previous MHD simulations (Dorelli et al., 2015; Jia et al., 2008, 2009b, 2010), we did not include any conductive ionosphere or inner boundary for Ganymede in our

Figure 1. Hybrid simulation results presented in the GphiO coordinate system. (a) Time snapshot of the global structure of Ganymede's magnetosphere when Ganymede is inside (G8 flyby) the Jovian plasma sheet. The horizontal plane is a 2D cut of the y-component of the electric current density, J_y, in the xy plane at $z = 0$. The vertical plane is a 2D cut of the parallel component of the electric current density to the magnetic fields, $J_\parallel$, in the yz plane at $x \approx +3.5R_G$. Magnetic field lines are traced in the xz plane, indicating (white) the Jovian magnetic field lines, (blue) closed magnetic field lines of Ganymede at low latitudes, (red) open magnetic field lines of Ganymede at high latitudes, and (green) recently reconnected magnetic fields. Ganymede is the gray sphere located in the middle of the figure. Part of the Galileo's trajectory during the G8 flyby is also marked by a solid line upstream of Ganymede. (b, c) Field-aligned current density during the G8 and G28 flybys in the yz plane at $x = 0$. The magnetic field lines are traced (black lines), and Ganymede is shown by a circle, centered at the origin of the coordinate system. The red color indicates currents flowing parallel to the field lines and the blue color shows the currents flowing antiparallel to the field lines. Magnitude of the electric current density for the G8 and G28 flybys (d, e) in the xy plane at $z = 0$ and (f, g) along the dashed lines shown in Figures 1d and 1e. The leading and trailing hemispheres are marked in Figures 1d and 1e. As shown by the directional arrows, the Jovian corotating plasma flows along the $+x$ axis and Jupiter is at the $+y$ axis. Ganymede is shown by a circle centered at the center of the coordinate system in Figures 1b–1e.

simulations. Therefore, the field-aligned currents do not close through any conductive layer close to Ganymede, and instead, they close through the magnetopause in our model. This indicates a major role that including any conductive boundary layer close to Ganymede plays in the closure of the field-aligned currents. However, the general structure of Ganymede's magnetosphere obtained from our simulations is similar to the previous modeling results (e.g., Dorelli et al., 2015; Fatemi et al., 2016; Jia et al., 2008, 2009b, 2010; Zhou et al., 2019).

Figures 1d and 1e show the magnitude of the electric current density in the xy plane at $z = 0$ during the G8 and G28 flybys, respectively, and Figures 1f and 1g show the electric current density along the white dashed lines shown in Figures 1d and 1e. Our simulations show that, regardless of Ganymede's location relative to the Jovian plasma sheet, the magnetopause stands at $\sim 1.85R_G$ upstream on the trailing hemisphere of Ganymede (i.e., $x = -1.85R_G$ in the GphiO coordinate system), which is consistent with Galileo observations (e.g., Kivelson et al., 1998) and previous simulations of Ganymede's magnetosphere (e.g., Dorelli et al., 2015; Fatemi et al., 2016; Jia et al., 2008, 2010; Zhou et al., 2020). Figures 1d and 1e show that the maximum current density at the magnetopause in the equatorial plane is ~ 0.7 μA/m^2. Our simulation results in different planes than those presented in this figure (not shown here) show that the upstream magnetopause current reaches to slightly over 1 μA/m^2. The magnetopause current, as explained later, effectively shields the surface of Ganymede at low latitudes from the incidence of the thermal plasma.

Figure 2 shows a time snapshot of the plasma density and bulk flow velocity obtained from our hybrid simulations when Ganymede is inside the Jovian plasma sheet (i.e., for the G8 flyby plasma conditions). Figures 2a and 2b show the normalized ion number density (n/n_0, where $n_0 = 8$ cm^{-3} is the corotating plasma density upstream of Ganymede) in the xy (at $z = 0$) and xz (at $y = 0$) planes, respectively. Figures 2c and 2d show the normalized x-component of the bulk flow velocity of all thermal ions (u_x/u_0, where $u_0 = 140$ km/s is the corotating plasma speed upstream of Ganymede) in the xy plane (at $z = 0$) and the z-component of the bulk flow velocity (u_z/u_0) in the xz plane (at $y = 0$), respectively. Figures 2e and 2f show the normalized plasma density and the x-component of the plasma velocity along the dashed lines shown in Figures 2a and 2c, but for the entire simulation domain along the x axis at $y = 0$ and $z = 0$.

As shown in Figure 2a, the plasma density is slightly higher than the upstream Jovian plasma density, n_0, and it increases to $\sim 2n_0$ upstream of Ganymede's magnetopause (Figure 2e), which is due to the propagation of compressional waves (not shown here). These upstream propagating electromagnetic perturbations (Kivelson et al., 2004), slow down the incident plasma and consequently, increase the plasma density (e.g., Jia et al., 2008). Figures 2c and 2f show the x-component of the plasma velocity at $x = -4R_G$ is nearly $0.7u_0$, and reduces to $0.5u_0$ upstream of the magnetopause ($x > -2.5R_G$), which is consistent with Galileo observations (Williams et al., 1998) and previous MHD simulations (e.g., Dorelli et al., 2015; Jia et al., 2008). The plasma flow stagnates along the x axis at the magnetopause ($x = -1.85R_G$ in Figure 2f) and as shown by arrows in Figures 2c and 2d, the flow is diverted around the magnetosphere of Ganymede. Figure 2b shows the closed magnetic field lines prevent the access of plasma to distances below $1.85R_G$, also evident from Figure 2e, forming a plasma cavity upstream on the trailing hemisphere.

In contrast to the upstream plasma cavity, the density inside the Alfvén wings and over the polar caps considerably increases (Figure 2b) to maintain conservation of mass and momentum (also see Fatemi et al., 2016). The arrow sizes in Figure 2d show the plasma flow speed inside the Alfvén wings substantially reduces to $\sim 0.2u_0$ (30 km/s) near the surface at high latitudes, which is consistent with Galileo observations and theoretical analysis (Williams et al., 1998; Vasyliūnas & Eviatar, 2000). As the flow convects downstream, it moves toward the central current sheet where magnetic reconnection occurs in the magnetotail ($+2R_G \lesssim x \lesssim +3R_G$, and $|z| \lesssim 0.3R_G$ in Figures 2b and 2d).

As shown in Figure 2d, the plasma flow is accelerated along the z axis at the magnetopause and its velocity reaches over $\pm 2u_0$ at $x \approx -1.85R_G$. There is also a north-south asymmetry in the z-component of the flow velocity at the magnetopause, which is primarily due to the slight tilt in the y-component of the Jovian magnetic field (see the upstream magnetic field lines in Figure 2b). This tilt moves the reconnection site above the equatorial plane for the time snapshot shown in Figure 2b.

Due to the diversion of the Jovian plasma around Ganymede's magnetosphere, the plasma density in the magnetotail substantially reduces to ~ 0.2–$0.3n_0$ (Figures 2a and 2e), except at distances smaller than $1.4R_G$ from the center of Ganymede on the leading hemisphere where the plasma density is comparable to the upstream Jovian

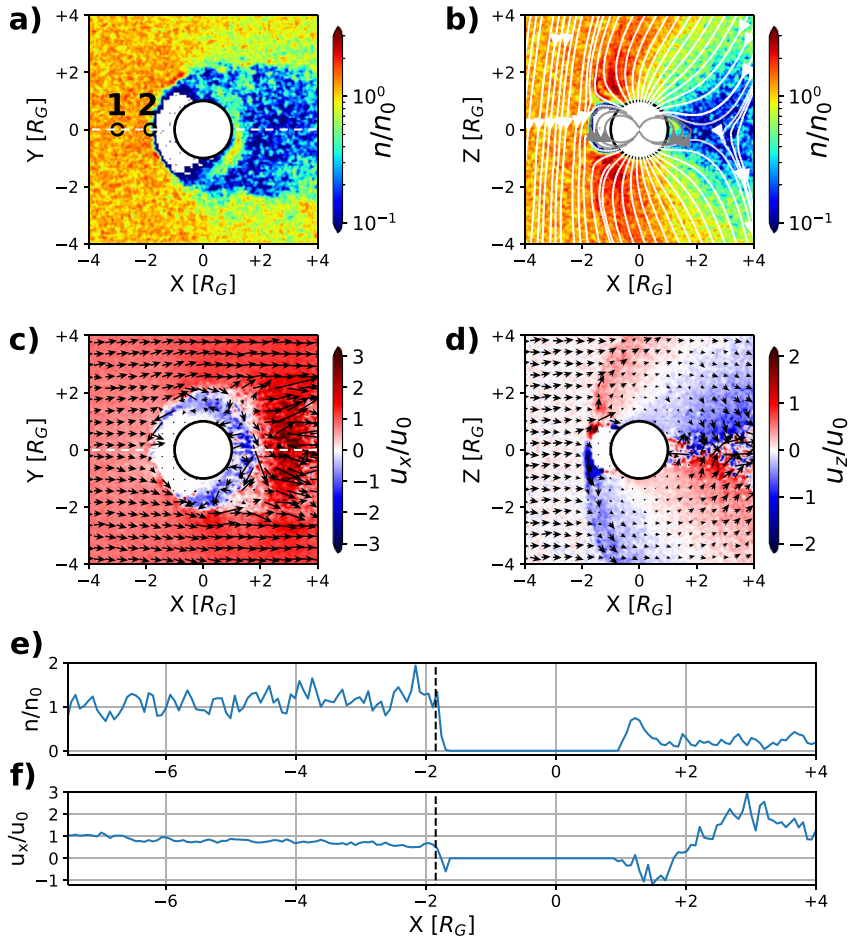

Figure 2. Hybrid simulation results during Galileo's G8 flyby presented in the GphiO coordinate system. (a, b) Total plasma number density normalized to the upstream Jovian plasma density $n_0 = 8$ cm^{-3}, (c, d) the x-component and z-component of the bulk flow velocity, normalized to the corotating plasma flow speed $u_0 = +140$ km/s, and (e, f) normalized plasma density and the x-component of the velocity along the dashed white lines shown in Figures 2a and 2c drawn for the entire simulation domain along the x axis. The vertical dashed lines in Figures 2e and 2f indicate the magnetopause location. Figures 2a and 2c are cuts in the xy plane at $z = 0$ and Figures 2b and 2d are cuts in the xz plane at $y = 0$. In Figure 2b, the open magnetic field lines are shown in white and the closed magnetic field lines are shown in gray. The directional arrows in Figures 2c and 2d show the direction of the plasma flow in the presented plane and the arrows sizes indicate the plasma flow speed. Ganymede is shown by a black circle, centered at the origin of the coordinate system. Two small black circles shown in Figure 2a indicate the area for particle selection in Regions 1 and 2 shown in Figure 6.

plasma density (Figure 2a). As shown in Figure 2c, there is a substantial increase in plasma flow velocity that moves away and toward Ganymede in the leading hemisphere which is due to the magnetic reconnection in the magnetotail that accelerates plasma away and toward Ganymede. The Ganymede-ward return flow, shown by blue color in Figure 2c, reaches to a maximum speed of $u_x \approx -1.0u_0$ at the center of the tail (e.g., see $x = +1.5R_G$ in Figure 2f). This flow partly impacts the surface of Ganymede on the leading hemisphere (Fatemi et al., 2016; Poppe et al., 2018), and partly gets diverted around the closed magnetic field lines on the leading hemisphere and moves upstream. Figure 2c shows that at the flanks of Ganymede's magnetosphere (i.e., $x \approx 0$ and $y = \pm 1.5R_G$) the plasma flows upstream with a speed of $\sim u_0$ along the $-x$ axis. Our simulations show that the return flow reaches the upstream magnetopause, evident by the directional arrows in Figure 2c at $x = -1.8R_G$ and by negative u_x/u_0 in Figure 2f near the upstream magnetopause. We discuss more about this return flow in Section 3.2.

In Figure 3, we show the structure of the electric field, power density, and the dominant electric field terms in Ganymede's magnetosphere and its surrounding plasma environment when Ganymede is inside the Jovian plasma sheet (i.e., during the G8 flyby). Figures 3a–3c show the magnitude of the normalized electric field ($|\mathbf{E}|/|\mathbf{E}_0|$, where $|\mathbf{E}_0| = 12.1$ mV/m is the convective electric field during the G8 flyby) in the xy (at $z = 0$), xz (at $y = 0$),

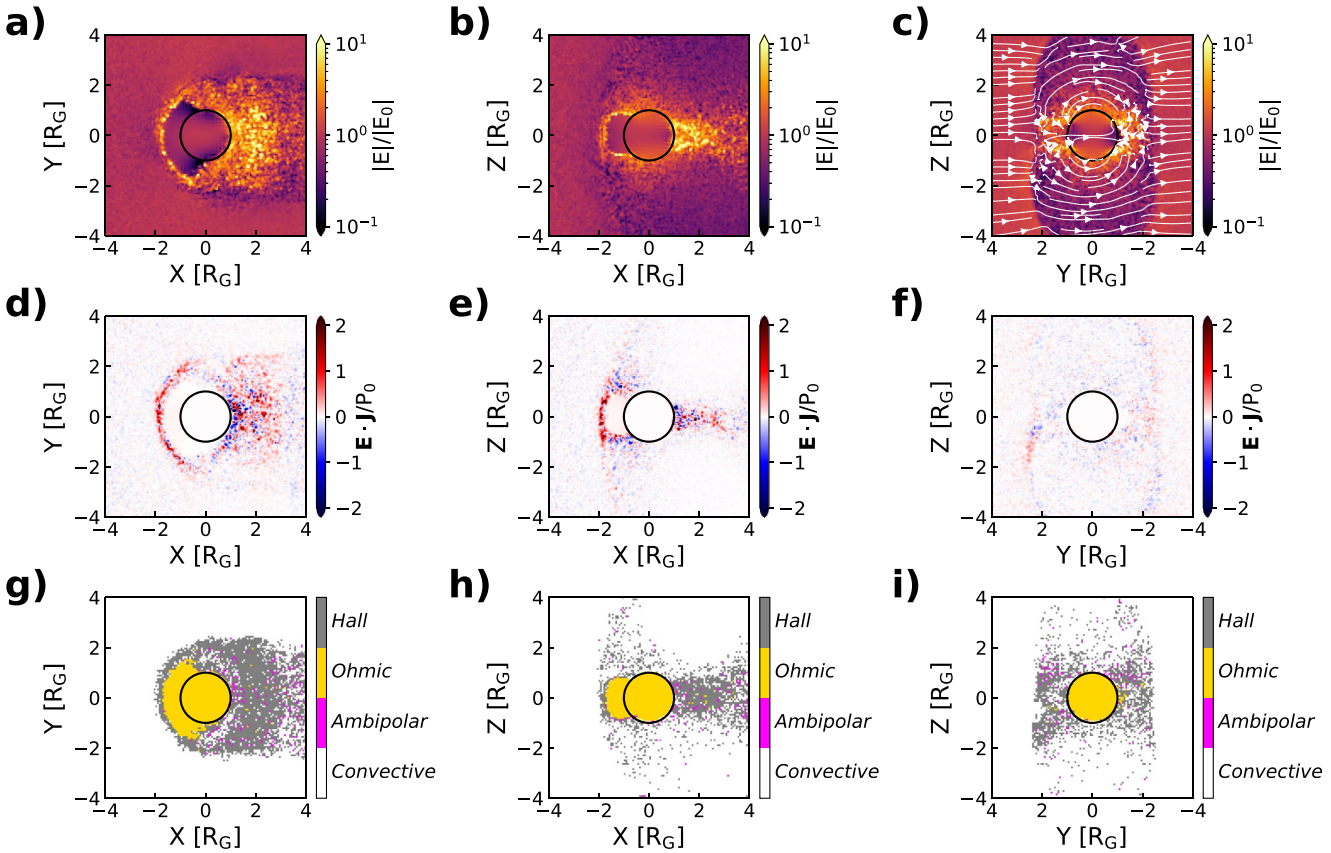

Figure 3. Hybrid simulation results when Ganymede is inside the Jovian plasma sheet presented in the GphiO coordinate system. (a–c) Background color shows the magnitude of the electric field normalized to the convective electric field of the corotating Jovian plasma, $E_0 = 12.1$ mV/m, and the electric field lines are shown by white lines in (c). (d–f) Power density, $\mathbf{E} \cdot \mathbf{J}$, normalized to $P_0 = 2.2$ nW/m^3. (g–i) Dominant electric field terms obtained from Equation 2. The left panels are cuts in the xy plane at $z = 0$, the middle panels are cuts in the xz plane at $y = 0$, and the right panels are cuts in the yz plane at $x = 0$. Ganymede is shown by a black circle, centered at the origin of the coordinate system.

and yz (at $x = 0$) planes, respectively. Figure 3a shows that the electric field increases to ~2–4E_0 at the upstream magnetopause, reaches to over 10E_0 downstream in the center of the magnetotail, and substantially reduces to ~0.3E_0 in the Alfvén wings.

Figures 3d–3f show the power density ($\mathbf{E} \cdot \mathbf{J}$) in the same plane as those for electric fields, normalized to $P_0 = 2.2$ nW/m^3, explained in Section 2.2. Positive/red (negative/blue) power density indicates regions that particles gain (lose) energy from (to) the electromagnetic fields. Figure 3d shows that the magnetopause has mainly a positive power density, which is expected, and thus the interacting particles with the magnetopause would mainly gain energy. The average power density of the entire magnetopause $P_{avg} \approx +0.95$ nW/m^3 (i.e., ~+0.45P_0), but the power density locally reaches to at highest ~+9P_0 and at lowest ~−3P_0 for our simulation setup and gird cell resolution. In the magnetotail, however, the power density is both positive and negative, especially at close distances to Ganymede on the leading hemisphere (Figure 3d), indicating conversion of energy from particles to fields. The average power density in the magnetotail is ~+0.2P_0, which is lower than that in the magnetopause, but the maximum (minimum) power density locally reaches to ~+78P_0 (~−6P_0), which is much stronger than that in the magnetopause.

Magnetospheric cusps can be identified from Figure 3e by the red/blue alternating region close to the surface at $x \approx -0.8R_G$ and $z \approx \pm 0.9R_G$. Particles that reach the cusps are expected to either mirror back or precipitate onto the surface of Ganymede, depending on their energy and pitch angle (the angle between the velocity vector and the local magnetic field). However, as shown previously in Figure 2d, the bulk flow of plasma in the cusp region at close distances to Ganymede is predominantly toward Ganymede's surface. It has been previously shown that a high flux of plasma impacts on the trailing hemisphere of Ganymede at the separatrix between the open and

closed field lines (Fatemi et al., 2016; Plainaki et al., 2015, 2020; Poppe et al., 2018). The power density in the *yz* plane (Figure 3f) is relatively weak in comparison to the magnetopause and magnetotail regions. However, the red/blue signatures outline the borders of the Alfvén wings.

The dominant electric field terms around Ganymede are shown in Figures 3g–3i. We calculated individual electric field terms from Equation 2, and for each grid cell, we found the maximum term along the total electric field in that grid cell. Figures 3g–3i show that in the ambient plasma outside Ganymede's magnetosphere as well as inside the Alfvén wings, the convective electric field (white area) is the dominant term. Inside Ganymede and in the low-density plasma regions (i.e., the plasma cavity between the magnetopause and Ganymede's surface), the Ohmic term (orange area) is the dominant electric field by our model construction. In Ganymede's magnetosphere, and particularly at the magnetopause and in the magnetotail, the Hall term (gray area) is the dominant electric field, which coincides well with regions of high-power density shown in Figures 3d–3f. The ambipolar electric field (pink area), which is related to the electron pressure gradient shown in Equation 2, has little or no dominance in Ganymede's magnetosphere on the scale of our simulation cell size. This can also be due to the lack of electron dynamics in hybrid simulations. A few of the previous MHD simulations have emphasized on the importance of the Hall electric field on the dynamics of Ganymede's magnetosphere, particularly at the magnetopause and magnetotail reconnection sites (Dorelli et al., 2015; Tóth et al., 2016; Zhou et al., 2020).

Except for the differences in the topology of the magnetosphere (e.g., see Figure 1), the overall structure and strength of the electric field and power density, and the dominant electric field terms when Ganymede is outside the Jovian plasma sheet (i.e., during the G28 flyby) are similar to those when Ganymede is inside the plasma sheet, thus not shown here. Our simulations (not shown here) suggest that the average power density at the upstream magnetopause when Ganymede is outside the plasma sheet is $P_{avg} \approx +0.75$ nW/m^3 (i.e., $\sim+0.4P_0$) and the power density locally reaches to at highest $+12P_0$ and at lowest $-6P_0$. Plasma β is smaller during the G28 flyby compared to that during the G8 flyby, but the magnetic shear angle between the Jovian and Ganymede magnetic fields at the magnetopause during the G28 flyby is much smaller than that during the G8 flyby. Therefore, the power density at the magnetopause when Ganymede is outside the plasma sheet is smaller than that when Ganymede is inside the plasma sheet.

3.2. Comparison With Galileo Observations

Figure 4 compares the magnetic fields between our hybrid simulations (red lines) and Galileo magnetometer observations (black lines) along the Galileo trajectories during the G8 (Figures 4a–4d) and G28 (Figures 4i–4l) flybys. The G8 flyby was the only Galileo's close encounter of Ganymede when Ganymede was close to the Jovian plasma sheet, whereas the G28 flyby is one of the five close encounters when Ganymede was outside the Jovian plasma sheet (Jia et al., 2008; Kivelson et al., 2004). We have selected these two flybys because they are the only ones that the Galileo spacecraft crossed the upstream side of Ganymede's magnetopause.

Figures 4a–4d and 4i–4l show a good agreement between our hybrid simulations and Galileo magnetometer measurements of the magnetic fields (Kivelson et al., 1998, 2002). Particularly, our model has captured the size and structure of the dayside magnetosphere during the two flybys. Our model has also reproduced sharp transitions during the magnetopause crossings (e.g., time ~15:52 UTC in Figure 4a and ~10:04 UTC in Figures 4j and 4k). Besides the good agreement, the major differences between our simulations and Galileo's magnetic field observations are the nearly 35 nT difference at closest approach to Ganymede during the G8 flyby (e.g., Figures 4a and 4d at time ~15:56 UTC) and a slight shift in the location of the outbound magnetopause crossing during the G28 flyby (e.g., Figure 4k between ~10:16 and ~10:18 UTC). In addition, our model is unable to capture a large enhancement in the B_y at time ~10:14 UTC during the G28 flyby (Figure 4j).

Galileo observed magnetic field fluctuations during the G8 inbound magnetopause crossing (around 15:52 UT). Kivelson et al. (1998) suggested the field fluctuations are associated with Kelvin-Helmholtz (KH) instabilities. Jia et al. (2010) using MHD simulations, however, showed that the fluctuations are a signature of an intermittent magnetic reconnection. As we explained in Section 3.1, our kinetic simulations presented in Figure 2c showed that a plasma flow returns from the magnetotail reconnection into the upstream magnetopause of Ganymede. The interaction between the return flow and the incoming Jovian plasma can potentially form KH instabilities at the magnetospheric flanks, which are not evident from our simulations, partly due to the low flux of the return flow, and partly due to the grid size effect in our simulations. Using smaller grid sizes is currently beyond the

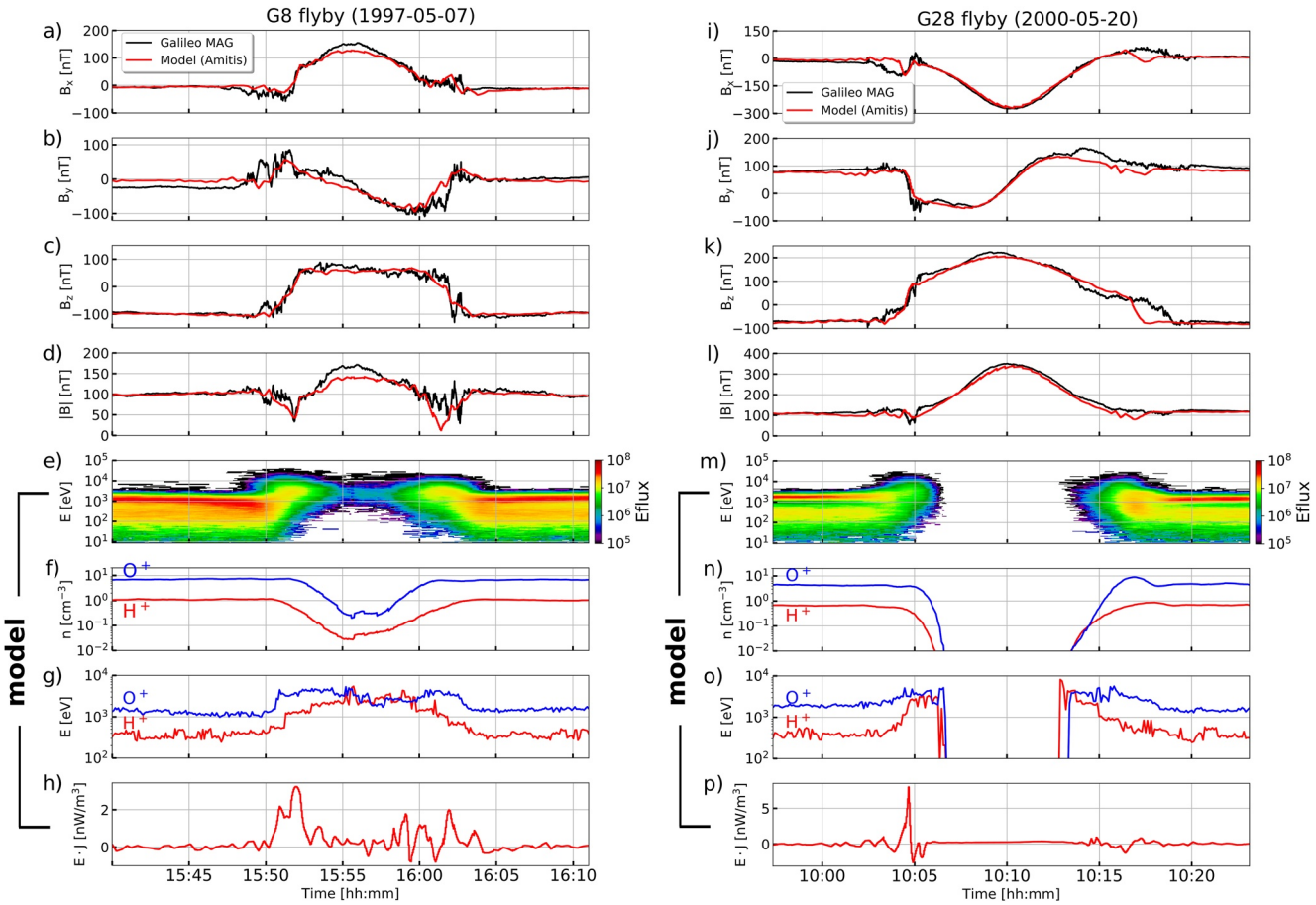

Figure 4. An overview of our hybrid simulations of the magnetic fields and plasma parameters (a–h) for the G8 and (i–p) for the G28 flybys along the trajectory of Galileo spacecraft for each flyby. The top four panels compare the magnetic fields between our hybrid simulations (red lines) and Galileo magnetometer observations (black lines). We also show our hybrid simulation results obtained along the trajectory of Galileo, showing (e, m) ion energy spectra where the differential energy fluxes ("Eflux") are in units of keV/cm^2/s/sr/keV, (f, n) ion density of (red) H^+ and (blue) O^+ ions, (g, o) ion bulk energy of (red) H^+ and (blue) O^+ ions, and (h, p) power density, $\mathbf{E} \cdot \mathbf{J}$.

computational limits of our global model, and thus the KH instabilities should be locally investigated using kinetic simulations. It is plausible that the field fluctuations are attributed to both the KH instabilities and magnetic reconnection, which requires further investigation and is beyond the scope of this study.

In addition to the magnetic fields, we also calculated the energy spectra (Figures 4e and 4m), the ion density (Figures 4f and 4n), and bulk energy (Figures 4g and 4o), and the power density (Figures 4h and 4p) from our hybrid simulations during the G8 and G28 flybys. Regardless of Ganymede's location relative to the Jovian plasma sheet, our simulations show that the energy of the corotating ions dramatically increases at the inbound and outbound magnetopause crossings due to the large power density. Figures 4e and 4m show that the ion energy reaches over 20 keV at the magnetopause crossings. The energy spectra during the G8 flyby (Figure 4e) is comparable to observations by the Galileo plasma science instrument (PLS; Frank et al., 1992) during that flyby, shown by Poppe et al. (2018).

During the G28 flyby, Galileo passed Ganymede at closer distances (the closest approach, CA, is $\sim 0.3R_G$ above the surface) than the G8 (CA $\approx 0.6R_G$) and moved into the closed field line region at the southern trailing hemisphere. During this period (between ~10:07 and ~10:12 UTC), neither the O^+, nor the H^+ ions moved into Ganymede's magnetosphere (Figure 4m), and as shown in Figure 4n, plasma density is zero in our simulations. During the G8 flyby, although Galileo passed the closed field line region at the northern trailing hemisphere, the plasma density substantially decreased (Figure 4f) but did not reach zero due to the higher altitude of Galileo compared to the G28 flyby. Comparing Figure 4g with Figure 4o, we see that the bulk flow energy of O^+ and H^+

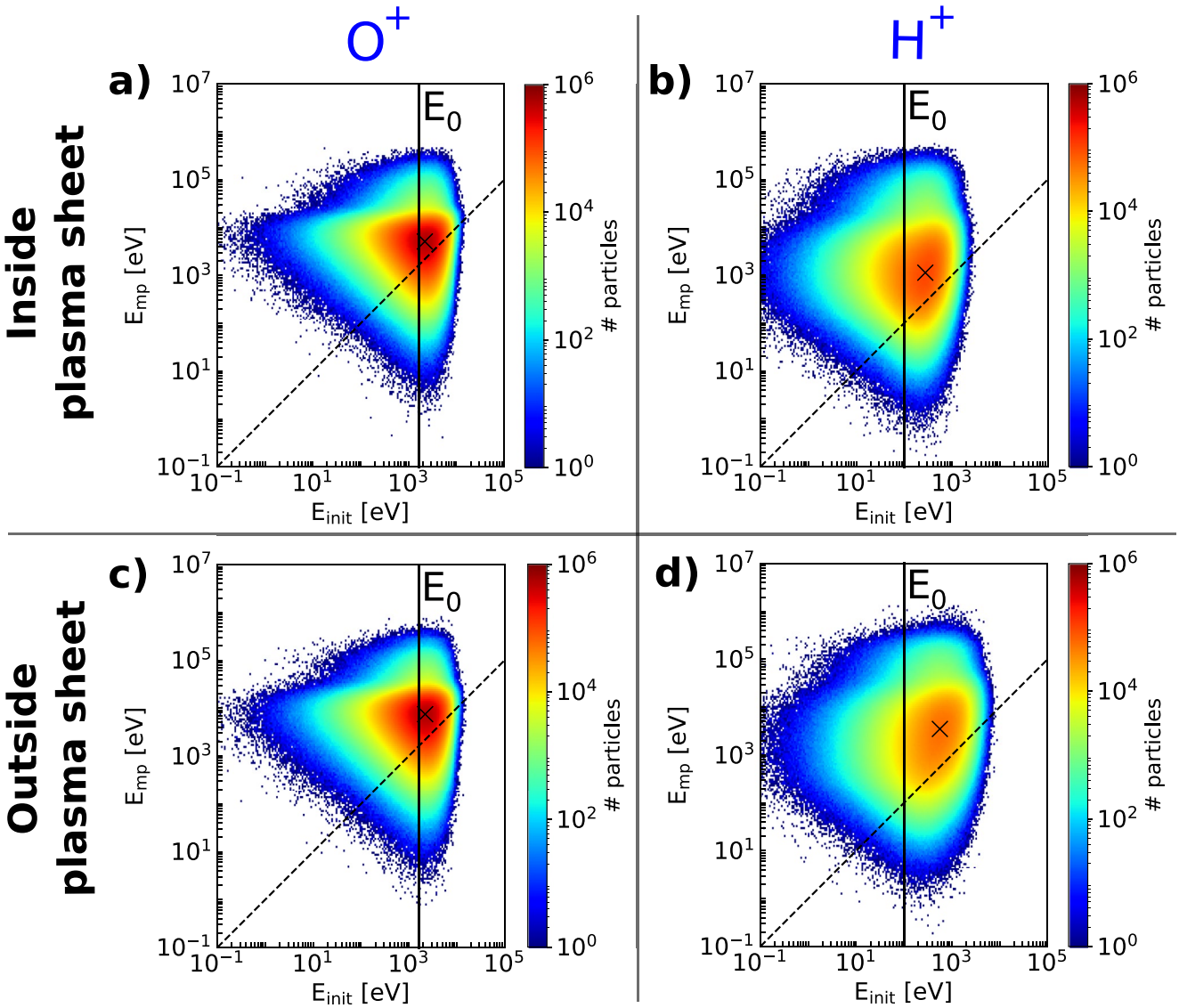

Figure 5. Two dimensional histograms for the correlation between the particles energy at initialization (i.e., at the inflow boundary of our simulations), E_{init}, and their energy when interacted with the upstream magnetopause of Ganymede, E_{mp}, obtained from our hybrid simulations (a, b) when Ganymede is inside the Jovian plasma sheet and (c, d) when Ganymede is outside the Jovian plasma sheet. Figures 5a and 5c show the energy distribution for O^+ ions and Figures 5b and 5d show the energy distribution for H^+ ions. The bulk energy of the ions applied to our simulations at the inflow boundary, E_0, is marked by the solid vertical lines, the direct relationship between E_{init} and E_{mp} is shown by the sloped dashed lines, and the peak of the distributions is indicated by crosses.

ions has substantially increased during the magnetopause crossings, but protons, due to their lighter mass, are more affected than the oxygen ions. We also see a large positive power density at both the inbound and outbound magnetosphere crossings during the G8 flyby (Figure 4h). This is in contrast to the simulations that suggest a large positive power density only at the inbound magnetospheric crossing for the G28 flyby, where the power density has drastically increased to 8 nW/m^3 (Figure 4p). The asymmetry in power density during the G28 flyby is due to the geometry of the flyby with respect to Ganymede's magnetosphere and the large y-component of the Jovian magnetic field (Figure 1c), which changes the structure of the magnetopause compared to the G8 flyby.

3.3. Plasma Interaction With Ganymede's Magnetopause

To better understand the dynamics of plasma interaction with Ganymede's magnetopause, we selected all the ions from our simulations that directly interacted with the magnetopause of Ganymede, as explained in Section 2.2. Figure 5 shows the energy distribution of O^+ and H^+ ions that interacted for the first time with the magnetopause

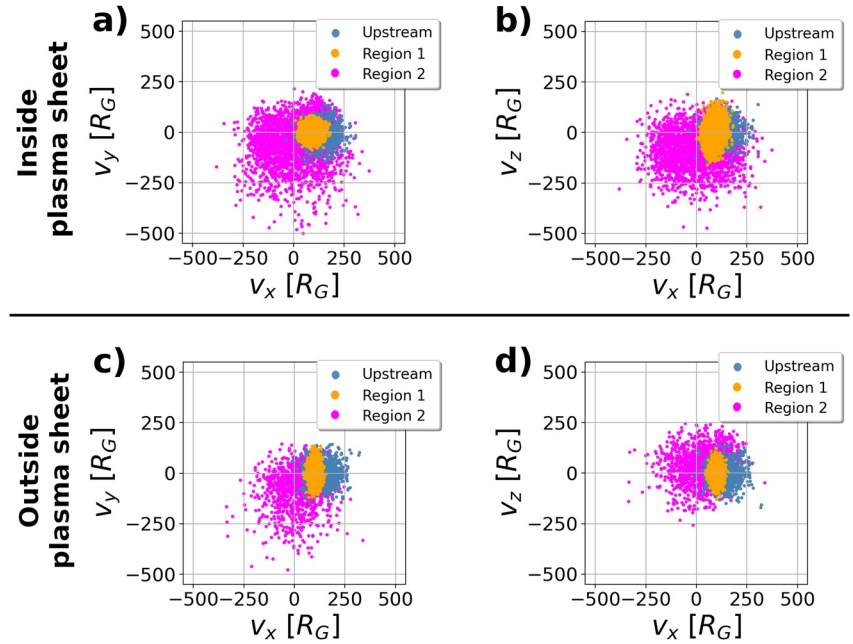

Figure 6. O^+ ions velocity distributions obtained from our hybrid simulations (a, b) when Ganymede is inside the Jovian plasma sheet and (c, d) when Ganymede is outside the Jovian plasma sheet. All particles are collected within a sphere of radius $0.2R_G$ (dark blue) upstream of Ganymede and away from magnetospheric perturbations centered at $(x, y, z) = (-7.5, +12, +12)R_G$, (orange) upstream of Ganymede's magnetopause, named as "Region 1," centered at $(x, y, z) = (-3, 0, 0)R_G$, and (pink) at the magnetopause, named as "Region 2," centered at $(x, y, z) = (-1.85, 0, 0)R_G$. Regions 1 and 2 are also marked by small black circles in Figure 2a. The particles in Region 2 are partly visible in this figure, because part of them is masked by the blue and orange dots.

(i.e., electric current density is higher than 0.2 μA/m^2 upstream of Ganymede, as explained in Section 2.2) when Ganymede is inside (Figures 5a and 5b) and outside (Figures 5c and 5d) the Jovian plasma sheet. The horizontal axes show the initial energy of the selected ions at the inflow boundary of our simulations, E_{init}, and the vertical axes show the energy of the particles when they interacted for the first time with the magnetopause, E_{mp} (see Section 2.2). The bulk energy of the ions applied to our simulations at the inflow boundary, E_0, is marked by the solid vertical lines, the direct relationship between E_{init} and E_{mp} is shown by the sloped dashed lines, and the peak of the distributions is indicated by crosses.

Figure 5 shows that, in general, most of the ions that interacted with the magnetopause have higher energies at the magnetopause than their initial energies (i.e., $E_{mp} > E_{init}$). In addition, our simulations show that the initial energy of the ions that interacted with the upstream magnetopause should be primarily higher than E_0. This is more pronounced for H^+ (Figures 5b and 5d) where the majority of the particles that reach the magnetopause have higher energies than E_{init}. Our simulations also show that a few of the initially very low-energy particles can interact with the magnetopause (i.e., $E_{init} < 10$ eV) with energies reaching $\sim 10^3$–10^4 eV for O^+ and $\sim 10^2$–10^4 eV for H^+ at the magnetopause. We see from Figure 5 that particles with a broad range of energies from $E_{mp} = \sim 1$ eV up to ~0.5 MeV interact with Ganymede's magnetopause. Due to a lower mass and consequently a smaller gyroradius, protons spend more time within the magnetopause, and thus more affected by the electric fields, compared to the oxygen ions.

Figure 6 shows the velocity distributions of O^+ ions when Ganymede is inside (Figures 6a and 6b) and outside (Figures 6c and 6d) the Jovian plasma sheet. Different colored-dots represent ion distributions at different locations including upstream of Ganymede and away from the magnetospheric disturbances (dark blue), upstream of the magnetopause named as Region 1 (orange), and at the magnetopause named as Region 2 (pink). All the particles are selected within a sphere of $0.2R_G$ in radius centered at $x = -7.5R_G$ and $(y, z) = +12R_G$ for the upstream region, $x = -3R_G$ and $(y, z) = 0$ for Region 1, and $x = -1.85R_G$ and $(y, z) = 0$ for Region 2. Regions 1 and 2 are marked by small black circles in Figure 2a.

The mean of the particles velocity for the upstream region (blue dots in Figure 6) when Ganymede is inside and outside of the plasma sheet is $(u_x, u_y, u_z) = (+139.3, -1.5, +0.5)$ km/s and (+141.4, −1.2, +1.8) km/s, respectively, and the particles distribution is Maxwellian with $T_{\parallel}/T_{\perp} \approx 1.0$ and a mean temperature of ∼218 eV, where $T_{\parallel}$ and $T_{\perp}$ are the parallel and perpendicular temperatures relative to the direction of the background Jovian magnetic field. All of these values are similar to those applied at the inflow boundary of our simulations. The O^+ ions in Region 1 are decelerated to a mean speed of ∼92 and ∼99 km/s when Ganymede is inside and outside the plasma sheet, respectively. Figure 6 shows that the velocity distribution in Region 1 is non-Maxwellian with plasma heating along the direction of the background Jovian magnetic field. When Ganymede is inside (outside) the Jovian plasma sheet, the background magnetic field is primarily along the z axis (y and z axes). Our analyses for Region 1 indicate that the O^+ ion velocity distribution exhibits $T_{\parallel}/T_{\perp} \approx 3.6$ (5.2) when Ganymede is inside (outside) the plasma sheet. The ion distribution at Region 2 (i.e., at the magnetopause) is also non-Maxwellian with thermal speeds of $(u_{thx}, u_{thy}, u_{thz}) \approx$ (103.8, 96.7, 85.5) km/s and (75.1, 84.9, 70.0) km/s, when Ganymede is inside and outside the plasma sheet, respectively. This clearly indicates that the O^+ ions are heated up to two times the thermal speed at the undisturbed upstream plasma (the thermal speed of the undisturbed Jovian plasma is ∼51 km/s along all directions). The mean particles velocity in Region 2 is $(u_x, u_y, u_z) \approx$ (+39.2, −26.6, −51.5) km/s and (+51.5, −38.5, +19.0) km/s, when Ganymede is inside and outside the plasma sheet, respectively. Figure 6 shows that a substantial fraction of the ions at the magnetopause (Region 2) move perpendicular to and against the direction of the corotating Jovian plasma.

Figure 7 shows the energy distribution of all O^+ and H^+ ions that interacted with the magnetopause and experienced a positive power density larger than P_0 (explained in Section 2.2) when Ganymede is inside the Jovian plasma sheet. Figures 7a and 7b show the energy distributions for the O^+ and H^+ ions, respectively, at the inflow boundary of our simulations, E_{init}, and the final energy of the particles when they impact the surface or leave our simulation domain, E_{final}. Comparing these two figures with Figures 5a and 5b, we see that the particles are further accelerated as they have passed through large positive power density regions in the magnetopause. Figures 7a and 7b show that the peak of the energy distributions, marked by crosses on the figures, is $(E_{\text{init}}, E_{\text{final}}) \approx$ (2.2, 18.0) keV and (0.27, 7.1) keV for the O^+ and H^+ ions, respectively. The peak of the energy distribution for these particles at initialization (i.e., ∼2.2 keV for the O^+ and ∼0.27 keV for the H^+ ions) is larger than the bulk initial energy of the corotating plasma applied to all particles at the inflow boundary of our simulations (i.e., ∼1.6 and ∼0.1 keV for the O^+ and H^+ ions, respectively, shown by the solid vertical lines). This indicates that, in general, larger energy than the bulk initial energy is required for the particles to interact with the high-power density regions in the magnetopause.

Figures 7c and 7d show the energy spectra of the ions that interacted with high-power density regions at the inflow boundary (solid blue line), at the first-time interaction with the upstream magnetopause (solid red line), at crossing a power density larger than P_0 in the magnetopause (dashed green line), and the final energy when leaving the simulation domain. We see from the difference between the peaks of the red and black curves in Figures 7c and 7d that the O^+ and H^+ ions are accelerated by ∼15.8 and ∼6.8 keV, respectively, after their interaction with the magnetopause. Figures 7e–7h show that the particles energy is mainly converted into the thermal energy at the magnetopause (red lines in Figures 7e and 7g), and then most of their final energy is converted into the parallel energy along the magnetic field lines (solid black lines in Figures 7f and 7h) after interacting with the high-power density regions.

Our simulations results for the O^+ and H^+ ions that crossed the magnetopause with a high positive power density, $P > P_0$, when Ganymede is outside the plasma sheet are presented in Figure 8, in the same format as those shown in Figure 7. Despite some similarities between the results presented in Figure 8 and those shown in Figure 7, there are a few fundamental differences in energy distributions and ion accelerations. For example, Figures 8a and 8b show that the peak of the energy distributions, marked by crosses on the figures, $(E_{\text{init}}, E_{\text{final}}) \approx$ (2.2, 27.6) keV and (0.56, 16.7) keV for the O^+ and H^+ ions, respectively. We also see from Figures 8c and 8d that the O^+ and H^+ ions are accelerated by ∼25.4 and ∼16.2 keV, respectively, after their interaction with the magnetopause. These indicate that both of the ion species are accelerated to much higher energies than those presented in Figure 7, which is due to the lower Alfvén Mach number and lower plasma β environment outside the Jovian plasma sheet compared to those inside the plasma sheet. In addition, our simulations show that the H^+ ions require relatively two times higher initial energies to reach the magnetopause when Ganymede is outside the plasma sheet (Figure 8b) compared to those when Ganymede is inside the plasma sheet (Figure 7b). Figure 8e also shows that when

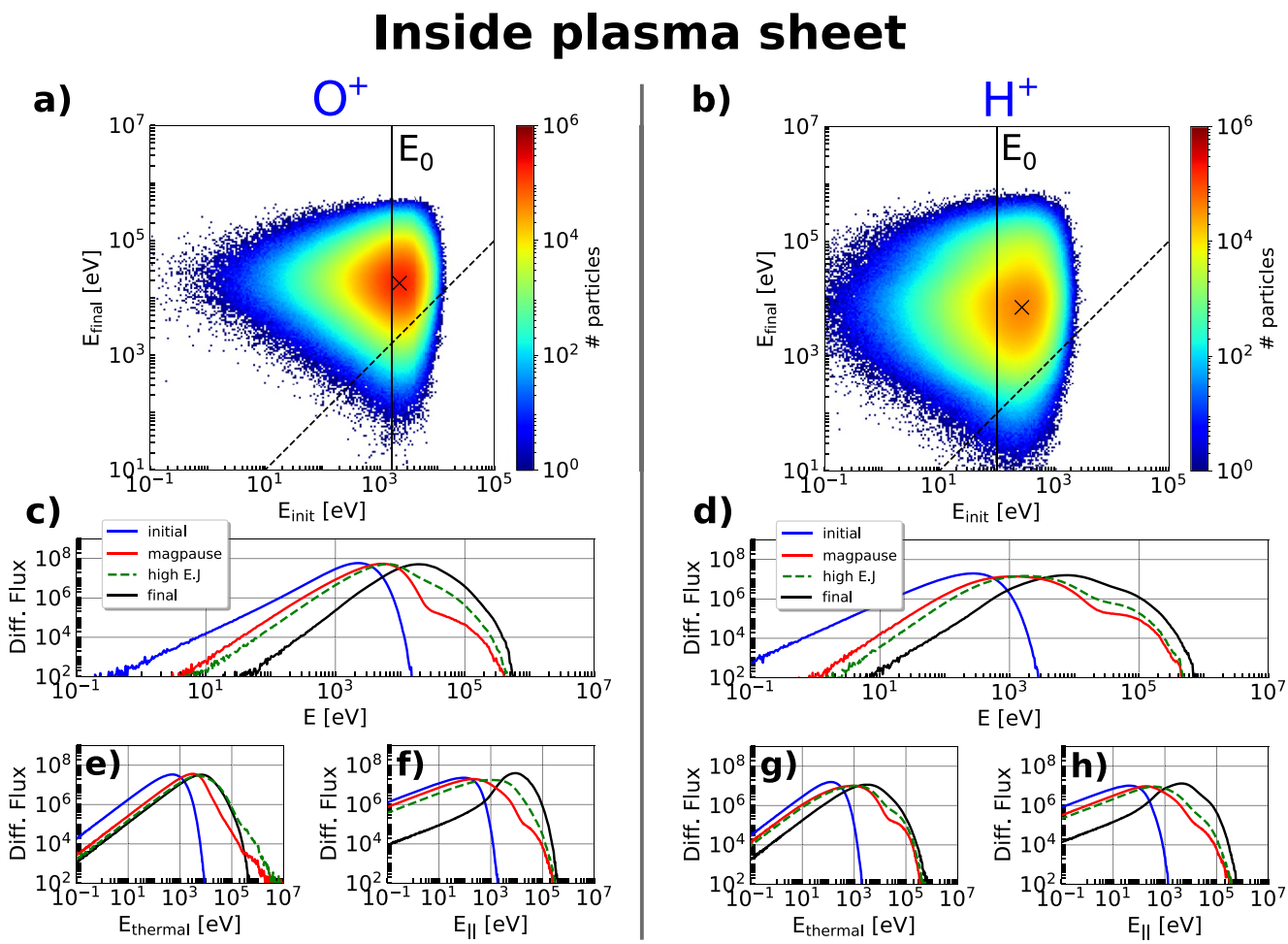

Figure 7. (a, b) Two dimensional histograms for the correlation between the particles energy at initialization (i.e., at the inflow boundary of our simulations), E_{init}, and their final energy, E_{final}, for all the particles that experienced a positive power density $P \geq P_0$ at the magnetopause crossing of Ganymede when Ganymede is inside the Jovian plasma sheet for (a) O^+ ions and (b) H^+ ions. (c) The differential flux distributions ($cm^{-2}\ s^{-1}\ sr^{-1}\ keV^{-1}$) as a function of energy for O^+ ions shown in Figure 7a, and (d) the differential flux distributions as a function of energy for H^+ ions shown in Figure 7b, for the particles (blue) upstream of Ganymede's magnetosphere, (red) at the upstream magnetopause, (dashed green) where $P \geq P_0$ at the upstream magnetopause, and (black) final location of the particles downstream of Ganymede's magnetosphere. The bottom panels are the differential flux distributions as a function of (e, g) thermal and (f, h) parallel energies for (e, f) O^+ ions, and (g, h) H^+ ions.

Ganymede is outside the plasma sheet the thermal energy of a considerable flux of O^+ ions reach over 1 MeV at the magnetopause crossing (solid red and dashed green lines).

In order to understand the interaction rate of O^+ and H^+ ions with the magnetopause of Ganymede and to provide estimates for the reconnection rate we selected all the particles that moved toward Ganymede's magnetosphere from the inflow boundary of our simulations (i.e., $x = -8R_G$ and $|y, z| \leq 2R_G$, which is equivalent to the size of the magnetosphere shown in Figure 1) and interacted with the magnetopause. For every 10 s of our simulations, Figure 9a shows the O^+ (circles) and H^+ (squares) ions interaction rate with the upstream magnetopause of Ganymede for the G8 (red) and G28 (blue) flybys. As shown in Figure 9a, during the first 30–40 s of our simulations, the number of upstream particles that reached the magnetopause is much higher than those at the later times. This is because the magnetosphere is in the development phase in our simulations and the fast mode compressional waves have not fully developed to deflect particles around the magnetosphere. Therefore, a large fraction of the Jovian plasma ions interacts with the developing magnetosphere of Ganymede.

After the simulations reached a steady state (i.e., time $t \geq 200$ s), on average ~22% of the upstream O^+ interact with the upstream magnetopause, regardless of Ganymede's location relative to the Jovian plasma sheet. Due to their lower mass, a large fraction of H^+ ions are diverted around the magnetosphere before reaching the magnetopause and thus, a much lower rate of H^+ ions interact with the upstream magnetopause. Since the magnetic field

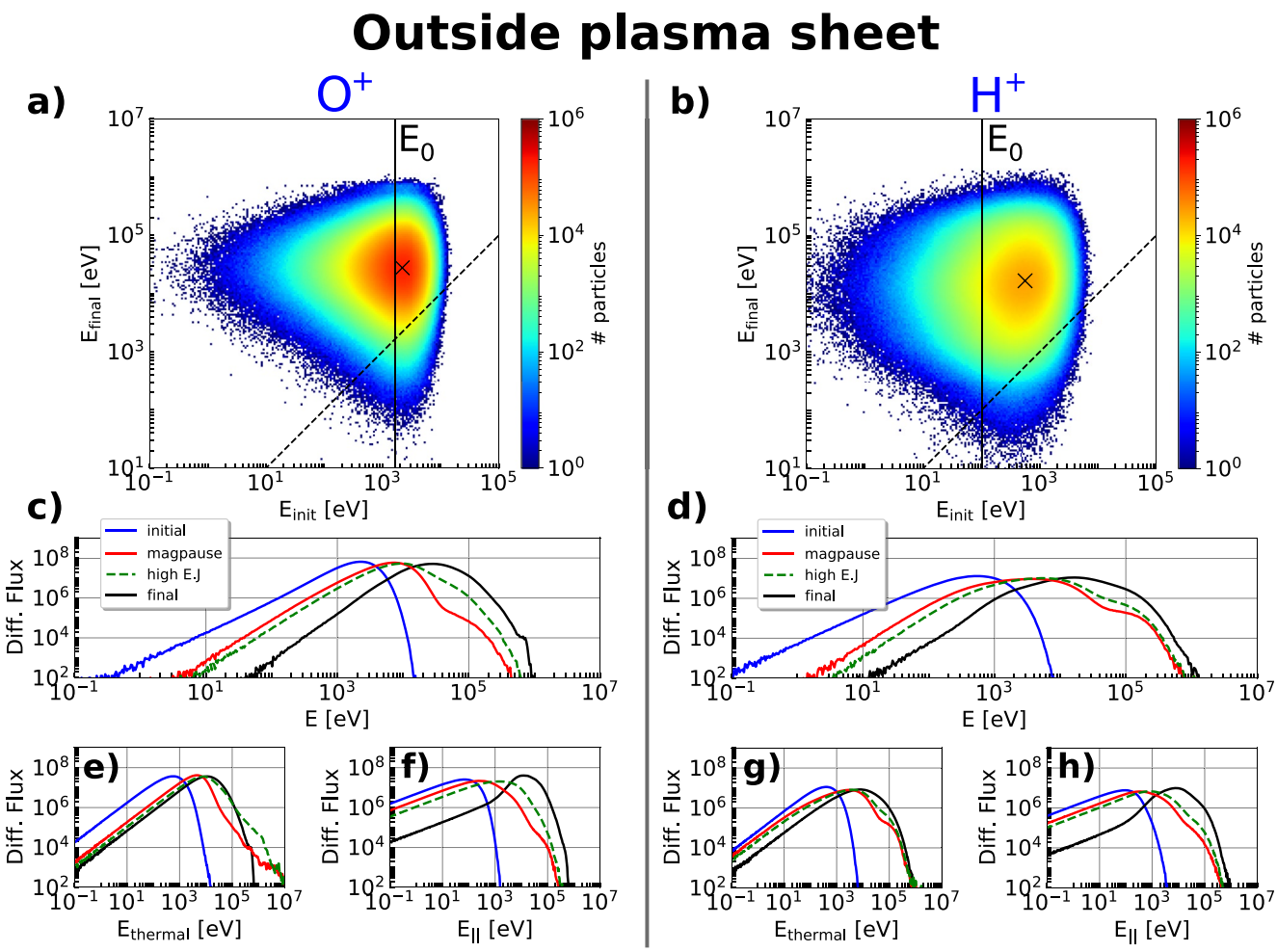

Figure 8. Energy distribution when Ganymede is outside the Jovian plasma sheet, presented in the same format as that shown in Figure 7.

intensity is higher when Ganymede is outside the Jovian plasma sheet (i.e., G28 flyby), the fast mode compressional waves propagating upstream of Ganymede deflect H^+ ions more effectively compared to heavier O^+ ions. Figure 9a shows that when Ganymede is inside (outside) the Jovian plasma sheet, on average ~9% (~6%) of the upstream H^+ ions interact with the upstream magnetopause.

Figure 9b shows the rate of the O^+ and H^+ ions that interacted with the magnetopause and experienced a large positive power density, $P \geq P_0$. After our simulations reached a steady state, on average ~(47 ± 7)% of the particles that have reached the magnetopause crossed a high-power density region. Figure 9b shows that the average interaction rate is ~3% higher when Ganymede is outside the plasma sheet.

Since the interaction environment during the two flybys has some fundamental differences, we also calculated the rate of the O^+ and H^+ ions that interacted with the magnetopause and experienced a positive power density larger than the average power density for each flyby (i.e., $P \geq +0.95$ nW/m^3 for the G8 flyby and $P \geq +0.75$ nW/m^3 for the G28 flyby), and the results are presented in Figure 9c. Our simulations show that, on average, ~(82 ± 6)% of the O^+ and H^+ ions crossed the magnetopause with $P \geq +0.95$ nW/m^3 during the G8 flyby, whereas ~(91 ± 10)% crossed $P \geq +0.75$ nW/m^3 during the G28 flyby. These suggest that the average reconnection rate at the magnetopause of Ganymede is ~82% and ~91% during the G8 and G28 flybys, respectively.

3.4. Examples of Charged Particle Motion

In this section, we show a few examples of particle trajectories that have interacted with Ganymede's magnetopause. Figure 10 shows an example of an O^+ ion trajectory that has interacted with the magnetopause when

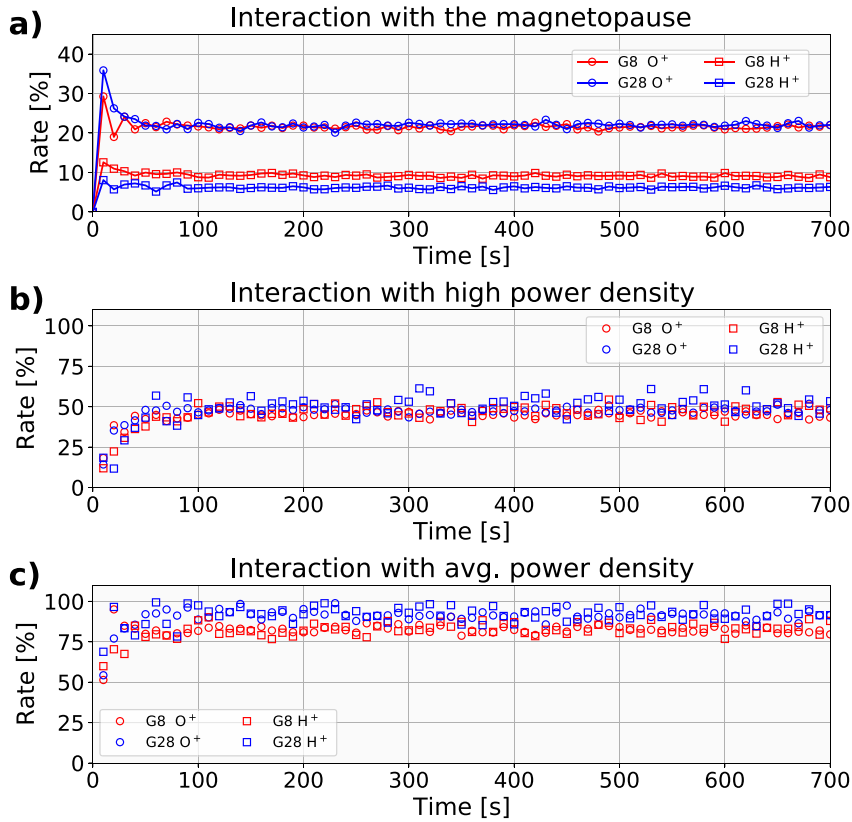

Figure 9. (a) The O^+ (circles) and H^+ (squares) ions interaction rate with the upstream magnetopause of Ganymede when Ganymede is inside (red) and outside (blue) the Jovian plasma sheet. (b) The rate of the O^+ and H^+ ions that interacted with the magnetopause and experienced a large positive power density $P \geq P_0$. P_0 for the G8 and G28 flybys is ∼2.2 and ∼2.0 nW/m^3, respectively. (c) The rate of the O^+ and H^+ ions that interacted with the magnetopause and experienced a positive power density $P \geq P_{avg}$, where P_{avg} = +0.95 nW/m^3 for the G8 flyby and P_{avg} = +0.75 nW/m^3 for the G28 flyby, explained in Section 3.1.

Ganymede is inside the Jovian plasma sheet. The background color in Figures 10a and 10b shows the intensity of the electric current density in the xy plane at $z = 0$ and in the xz plane at $y = 0$, respectively. A projection for a part of the ion trajectory on each plane is also shown in these figures and the color indicates the energy of the particle along its trajectory. The initial velocity of the selected particle at the inflow boundary of our simulation is ($v_{x_{init}}$, $v_{y_{init}}$, $v_{z_{init}}$) = (+159.2, +2.4, +19.2) km/s, which is equivalent to an initial energy of ∼2.1 keV. The final velocity of this particle is ($v_{x_{final}}$, $v_{y_{final}}$, $v_{z_{final}}$) = (+309.5, +146.6, +339.4) km/s, which corresponds of an energy of ∼19.2 keV. As shown in Figure 7, the 2 keV initial energy and 19 keV final energy correspond to the peak of the energy distribution for O^+ ions. Therefore, the selected particle trajectory is a *typical* example of the O^+ ion trajectory that interacted with the magnetopause of Ganymede. In this example, the ion has interacted with the magnetopause and moved along the northern Alfvén wing.

Figure 10c shows the three components of the magnetic fields that the particle has experienced along its trajectory. At time t = 153 s, the particle has reached the upstream magnetopause where the magnetic field is nearly zero. Nearly at that time the particle experiences a large power density P = +5.8 nW/m^3, shown in Figure 10d, which is nearly 2.5P_0. We see from Figure 10e that during the magnetopause crossing period (i.e., between ∼153 and ∼156 s), the z-component of the particle's velocity, v_z, dramatically increases from a few 10s of km/s to nearly +375 km/s, while the v_x decreases to nearly zero and the v_y reaches to ∼−170 km/s. We also see from Figures 10a and 10b that the particle has changed its direction of motion toward $+z$ and $-y$ after interacting with the magnetopause. Figure 10g shows that the particle's thermal and parallel speeds have also increased at the magnetopause, but most of the particle's energy has been converted into the thermal energy during the interaction with the magnetopause. A few seconds later, the parallel energy of the particle overtook the thermal energy and the parallel speed has increased to ∼−430 km/s as the particle moves in the opposite direction to the magnetic field lines in

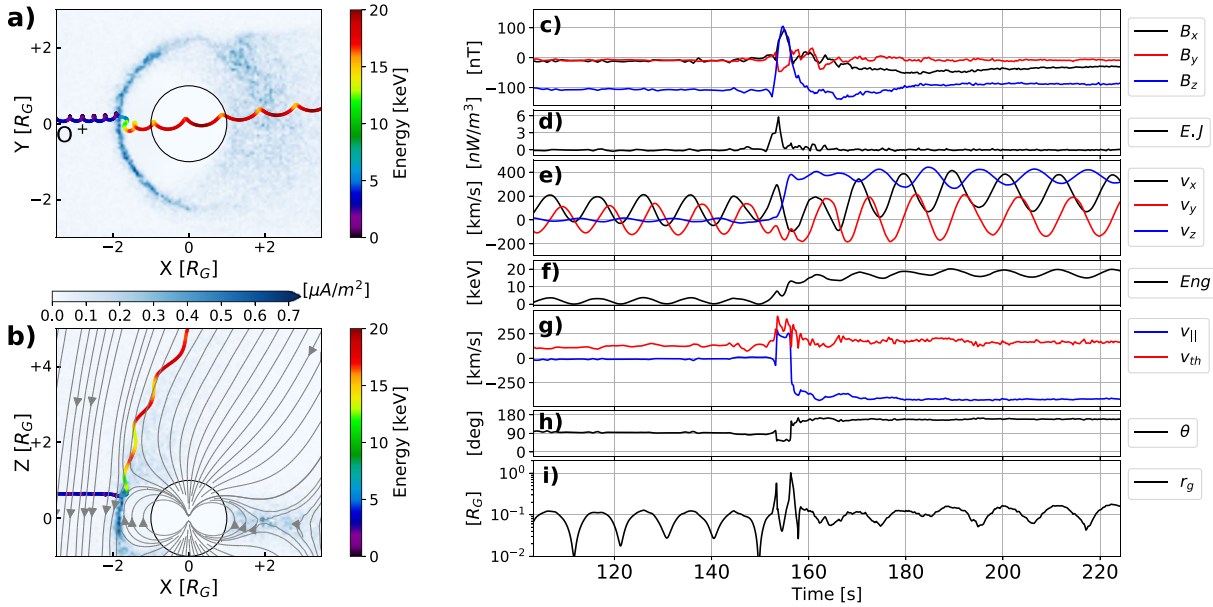

Figure 10. An example of a typical O^+ ion trajectory that interacts with Ganymede's magnetopause when Ganymede is inside the Jovian plasma sheet obtained from our hybrid simulations projected into (a) *xy* plane at $z = 0$ and (b) *xz* plane at $y = 0$, where the background blue color shows the magnitude of the electric current density, and the color along the particle's trajectory shows the particle's energy. In Figure 10b, the magnetic field lines are shown in gray and Ganymede is shown by a black circle, centered at the origin of the coordinate system. (c) Three components of the magnetic fields, (d) power density, (e) three components of the ion velocity, (f) total ion energy, (g) the thermal and parallel components of the velocity, (h) particle's pitch angle, and (i) particles gyroradius, as a function of time, obtained along the trajectory of the selected O^+ ion.

the northern Alfvén wing. The selected particle has interacted with the closed magnetic field lines of Ganymede on the trailing hemisphere before moving into the Alfvén wings, and therefore, its parallel speed has turned positive after the particle has interacted with the magnetopause. We can also see this in the particle's pitch angle shown in Figure 10h. Figure 10i shows that the gyroradius of the selected O^+ ion is $\sim 0.1 R_G$ before it reaches the upstream magnetopause. At the magnetopause, however, the particle's gyroradius becomes comparable or even slightly larger than $1 R_G$ for a short period of time. In the northern Alfvén wing and downstream of Ganymede's magnetosphere, the O^+ gyroradius is $\sim 0.2 R_G$.

Figure 11 shows an example of a *typical* trajectory for an H^+ ion that interacted with the magnetopause of Ganymede and experienced a large positive power density, and presented in the same format as that shown in Figure 10. The initial velocity of the selected ion at the inflow boundary of our simulations is ($v_{x_{init}}$, $v_{y_{init}}$, $v_{z_{init}}$) = (+216.0, +4.7, −13.4) km/s, which corresponds to an initial energy of ∼0.24 keV. The final velocity of the particle when leaving our simulation domain is ($v_{x_{final}}$, $v_{y_{final}}$, $v_{z_{final}}$) = (+298.0, −374.4, −757.3) km/s, which corresponds of an energy of ∼4.1 keV. We selected this particle because it experienced a power density at the magnetopause relatively similar to the O^+ ion shown in Figure 10, thus their energy gain can be compared. Due to the lighter mass, the H^+ ion has a much shorter gyroperiod (e.g., see Figure 11e) and smaller gyroradius (Figure 11i) compared to the O^+ ion. In addition, the energy gain for the H^+ ion after interaction with the magnetopause is nearly 2 times higher than that for the O^+ ion.

Certainly, the interaction of all the ions shown in Figures 5–7 are not as simple as those presented in Figures 10 and 11. For example, we see from Figure 7a that particles with similar initial energies may have a broad range of final energies, much larger than their initial energies, thus should have interacted differently with the magnetosphere than the *typical* ions. Figure 12 shows an example trajectory of an O^+ ion with an initial velocity at the inflow boundary of our simulation of ($v_{x_{init}}$, $v_{y_{init}}$, $v_{z_{init}}$) = (+136.7, +0.2, +12.1) km/s (i.e., E_{init} = 1.6 keV) and a final velocity of ($v_{x_{final}}$, $v_{y_{final}}$, $v_{z_{final}}$) = (+441.2, +1362.2, +759.0) km/s (i.e., E_{final} = 217 keV). The initial position of this particle is ($r_{x_{init}}$, $r_{y_{init}}$, $r_{z_{init}}$) = (−8.0, +0.23, +0.13)R_G. The initial energy and velocity of the selected particle is very close to the bulk initial energy and velocity of the corotating Jovian plasma. Therefore, it is expected that the particle has a similar trajectory to the ion shown in Figure 10. However, the energy gain for this particle after interaction with the magnetosphere of Ganymede is dramatically higher than that shown in Figure 10.

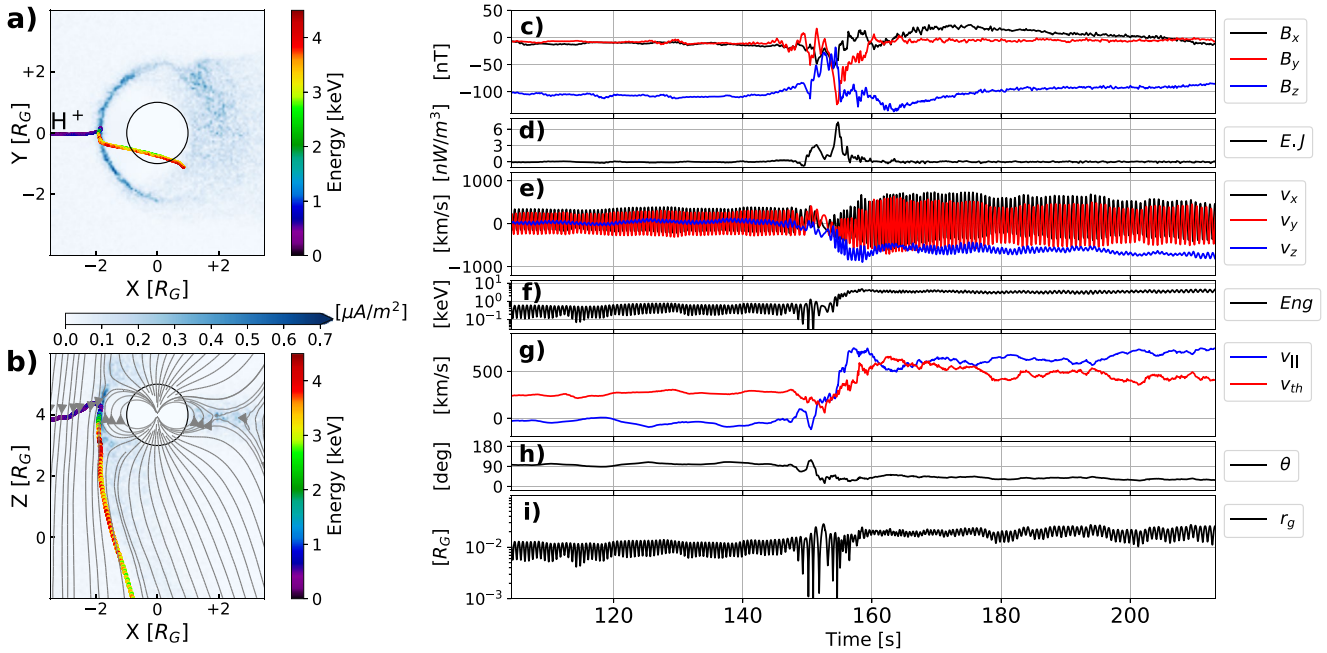

Figure 11. An example of a typical H^+ ion trajectory that interacts with Ganymede's magnetopause when Ganymede is inside the Jovian plasma sheet obtained from our hybrid simulations. The figure format is the same as that shown in Figure 10.

As shown in Figure 12b and as can be also seen from Figures 12c and 12d, the particle has interacted with the upstream magnetopause at time $t = 153$ s where the power density is close to $P_0 = 2.2$ nW/m^3. The particle's energy has slightly increased to 9 keV (Figure 12f at $t = 153$ s) and its gyroradius became comparable to the size of Ganymede (Figure 12i). After that, the particle has moved closer to Ganymede and entered the northern magnetospheric cusp at $t = 159$ s. We see from Figure 12h that the local pitch angle of the particle is 90° at $t = 160$ s where the particle is mirrored back and moved upstream of Ganymede with a large gyroradius (Figure 12i) and a

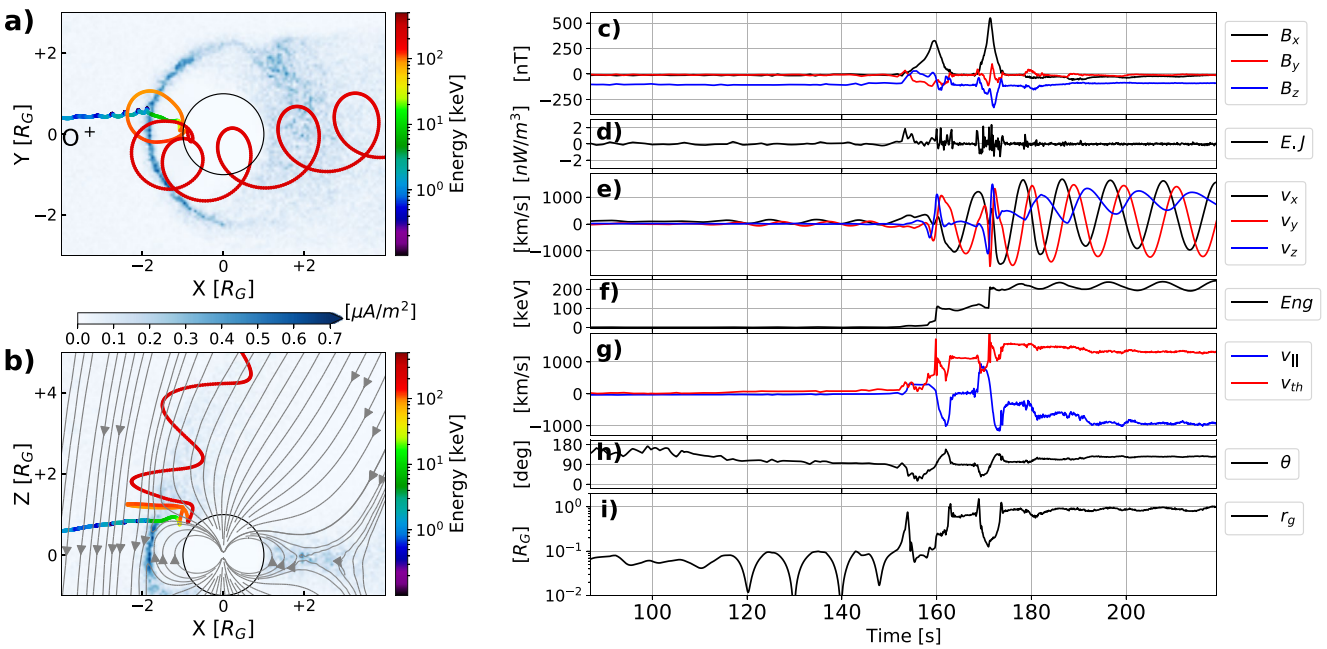

Figure 12. An example of an O^+ ion trajectory that interacts with Ganymede's magnetopause and gains an energy over two orders of magnitude from its initial energy. The figure format is the same as that shown in Figure 10.

high energy (~100 keV, shown in Figure 12f). After the first interaction with the magnetosphere, the particle has moved again into the cusp at $t = 171$ s and its energy has increased by a factor of two. As shown in Figures 12a and 12b, the particle has moved downstream with a relatively stable energy and its gyroradius is comparable to the size of Ganymede.

4. Discussion and Conclusion

We used a multi-GPU version of the Amitis hybrid-kinetic model of plasma to study ion dynamics at Ganymede's magnetopause when Ganymede is inside and outside the Jovian plasma sheet. The global structure of Ganymede's magnetosphere obtained from our simulations and presented in Figures 1–3 is in general agreement with previous MHD and hybrid simulations (e.g., Dorelli et al., 2015; Fatemi et al., 2016; Jia et al., 2008, 2010; Paty & Winglee, 2004; Tóth et al., 2016; Zhou et al., 2019, 2020) including the formation of the magnetopause at $1.85R_G$ upstream of Ganymede, the size of the magnetosphere which is $\sim 4R_G$ at $x = 0$ and expands to $\sim 6R_G$ downstream, the formation of the Alfvén wings, and magnetic reconnection upstream and downstream of Ganymede.

We also successfully compared our hybrid simulation results with Galileo's magnetometer and PLS observations (Figure 4). We found an excellent agreement between our simulations and observations, especially with the magnetic field observations. Figure 4 shows that our model is capable of correctly capturing the magnetopause of Ganymede. Particularly during the G8 flyby, our model has reproduced the size of the magnetosphere and fully presented a sharp transition during the inbound magnetopause crossing.

Previously, Fatemi et al. (2016) used a hybrid model of plasma to explain asymmetries in brightness patterns on Ganymede's surface and compared their simulations with all the six Galileo flybys. Except the size of the magnetosphere and sharp transitions during the G8 magnetopause crossings, they found a good agreement between their hybrid simulations and observations. Since the principles of the hybrid model in the Amitis code used in this study and those used by Fatemi et al. (2016) are similar with only slight differences in numerical solvers and high performance computing techniques, we conclude that the reasons for significant improvements in the simulation results obtained from the Amitis code, particularly for the G8 flyby, besides differences in the numerical methods, might be due to either or all of the following reasons: (a) we used a higher plasma density in this study, which plays a crucial role in changing the size and structure of the magnetosphere, (b) we substantially improved particle statistics using the multi-GPU version of the Amitis code, (c) we applied multiion species with more realistic representation of the Jovian plasma environment in this study, and (d) we used a higher simulation grid resolution compared to those used by Fatemi et al. (2016).

Ganymede's magnetosphere, as shown in our hybrid simulations presented in Figures 1–3, is small relative to the size of Ganymede and most of the magnetosphere is filled in by the body of the moon itself. In such a small magnetosphere, ion gyroradius scale is comparable to the size of the magnetosphere, especially for heavy ions that interact with the magnetopause (e.g., Figure 12i). Moreover, every individual particle in Ganymede's magnetosphere undergoes a set of particle drifts, such as $E \times B$, grad-B, and curvature drift motions (Poppe et al., 2018). Due to the small size of Ganymede's magnetosphere and large ion gyroradius, the interaction of ions with Ganymede leads to formation of a complex and kinetic interaction (Dorelli et al., 2015; Fatemi et al., 2016; Poppe et al., 2018). In addition, velocity distributions of ions that reached the magnetosphere of Ganymede (Region 1), and interacted with the magnetopause (Region 2) are highly non-Maxwellian (Figure 6), a feature that violates MHD assumptions. Therefore, as also suggested previously by Dorelli et al. (2015), kinetic effects of ions play a major role in the dynamics of the magnetosphere.

It was previously shown by Dorelli et al. (2015) that resistive MHD cannot capture the global structure and dynamics of Ganymede's magnetosphere, and a Hall-MHD (with the inclusion of the Hall term) is required (Tóth et al., 2016; Zhou et al., 2020). In contrast to both resistive MHD and Hall-MHD models, we used a hybrid-kinetic model of plasma that treats ions as particles. Our simulations presented in Figure 3 show that the Hall term is the most dominant term in the entire magnetosphere of Ganymede, confirming previous emphasis on the importance of the Hall effects. In addition, the high thermal energy of the O^+ ions at the magnetopause (e.g., Figure 7e) indicates that a gyro-center approximation, or in other words, fluid approximation, cannot describe the dynamics of these ions in the magnetosphere of Ganymede. However, this statement is not valid for H^+ ions (Figure 7g), which can be well represented by a fluid approximation due to their small gyroradius (Figure 11i).

Thus, we conclude that the interaction between the Jovian plasma and Ganymede's magnetosphere needs to be modeled kinetically for ions heavier than H^+ ions.

Due to the large shear angle between the Jovian magnetic fields and Ganymede's intrinsic magnetic fields, and the low Alfvén Mach and low plasma β environment of Ganymede, magnetic reconnection is a major process that takes place at Ganymede's magnetopause and magnetotail. Our hybrid simulations result showed that the Hall term is the dominant electric field component at the magnetopause (e.g., Figure 3g) and the power density is predominantly positive, with $P > P_0$ (e.g., Figure 3d), which is an indication of magnetic reconnection. The reconnection at the upstream magnetopause is suggested to be intermittent, leading to the formation of flux transfer events (FTEs; Jia et al., 2010; Tóth et al., 2016; Zhou et al., 2020). Recently, Zhou et al. (2020) using MHD and MHD-EPIC simulations developed a model to calculate the global magnetic reconnection rate at Ganymede. Their model estimated the rate at the upstream magnetopause is about 80 kV with 60% efficiency. Our analysis from our kinetic simulations (Figure 9) show that ≈47% of the incident Jovian ions cross the magnetopause and experience a high positive power density, $P \geq P_0$. While this rate is slightly higher when Ganymede is outside the Jovian plasma sheet, the difference (∼2–3%) is not considerably high compared to those when Ganymede is inside the plasma sheet. Although the criteria for selection of particles crossing a high-power density region $P \geq P_0$ is an indication for particle crossing through a region that has enough power to divert particles within the time frame of one gyroradius, and thus, is applicable for indication of the magnetic reconnection rate, we also examined $P \geq P_{avg}$ and we concluded ≈82% and ≈91% of the particles crossed the magnetopause with $P \geq P_{avg}$ during the G8 and G28 flybys. This suggests that the reconnection rate in our simulations for $P \geq P_{avg}$ is higher than the 60% efficiency estimated by Zhou et al. (2020), but in general is consistent with their estimations.

Data Availability Statement

All Galileo data used here are publicly available at NASA's Planetary Data System (PDS). The simulation results are publicly available online at https://doi.org/10.5281/zenodo.5171314.

Acknowledgments
S. F., A. V., and J. L. acknowledge support from the Swedish National Space Agency (SNSA), Grant 179/18. S. F. also acknowledges supports from SNSA Grant 115/18, and the Swedish Research Council (VR) Grant 2018-03454. J. L. also acknowledges support from the Royal Swedish Academy of Sciences (KVA) foundations through stipend AST2020-0011. A. R. P. acknowledges support from NASA SSW Grant NNX16AR99G. The computations were partly enabled by resources provided by the Swedish National Infrastructure for Computing (SNIC) at the High Performance Computing Center North (HPC2N), Umeå University, Sweden. In addition, the corresponding author acknowledges support from NVIDIA's Academic Hardware Grant Program that facilitated in-house running of our simulations and helped us to advance our model toward a multi-GPU model.

References

Acuna, M. H., & Ness, N. F. (1976). The main magnetic field of Jupiter. *Journal of Geophysical Research*, *81*(16), 2917–2922. https://doi.org/10.1029/JA081i016p02917

Bagenal, F., & Delamere, P. A. (2011). Flow of mass and energy in the magnetospheres of Jupiter and Saturn. *Journal of Geophysical Research*, *116*, A05209. https://doi.org/10.1029/2010JA016294

Bagenal, F., Wilson, R. J., Siler, S., Paterson, W. R., & Kurth, W. S. (2016). Survey of Galileo plasma observations in Jupiter's plasma sheet. *Journal of Geophysical Research: Planets*, *121*, 871–894. https://doi.org/10.1002/2016JE005009

Belcher, J. W. (1983). The low energy plasma in the Jovian magnetosphere. In A. J. Dessler (Ed.), *Physics of the Jovian magnetosphere* (Chap. 3). Cambridge University Press. https://doi.org/10.1017/cbo9780511564574.005

Collinson, G., Paterson, W. R., Bard, C., Dorelli, J., Glocer, A., Sarantos, M., & Wilson, R. (2018). New results from Galileo's first flyby of Ganymede: Reconnection-driven flows at the low-latitude magnetopause boundary, crossing the cusp, and icy ionospheric escape. *Geophysical Research Letters*, *45*, 3382–3392. https://doi.org/10.1002/2017GL075487

Cooper, J. F., Johnson, R. E., Mauk, B. H., Garrett, H. B., & Gehrels, N. (2001). Energetic ion and electron irradiation of the icy Galilean satellites. *Icarus*, *149*(1), 133–159. https://doi.org/10.1006/icar.2000.6498

Dorelli, J. C., Glocer, A., Collinson, G., & Tóth, G. (2015). The role of the Hall effect in the global structure and dynamics of planetary magnetospheres: Ganymede as a case study. *Journal of Geophysical Research: Space Physics*, *120*, 5377–5392. https://doi.org/10.1002/2014JA020951

Duling, S., Saur, J., & Wicht, J. (2014). Consistent boundary conditions at nonconducting surfaces of planetary bodies: Applications in a new Ganymede MHD model. *Journal of Geophysical Research: Space Physics*, *119*, 4412–4440. https://doi.org/10.1002/2013JA019554

Dungey, J. W. (1961). Interplanetary magnetic field and the auroral zones. *Physical Review Letters*, *6*(2), 47–48. https://doi.org/10.1103/physrevlett.6.47

Fatemi, S., Poppe, A., & Barabash, S. (2020). Hybrid simulations of solar wind proton precipitation to the surface of mercury. *Journal of Geophysical Research: Space Physics*, *125*, e2019JA027706. https://doi.org/10.1029/2019JA027706

Fatemi, S., Poppe, A. R., Delory, G. T., & Farrell, W. M. (2017). Amitis: A 3D GPU-based hybrid-PIC model for space and plasma physics. *Journal of Physics: Conference Series*, *837*, 012017. https://doi.org/10.1088/1742-6596/837/1/012017

Fatemi, S., Poppe, A. R., Khurana, K. K., Holmström, M., & Delory, G. T. (2016). On the formation of Ganymede's surface brightness asymmetries: Kinetic simulations of Ganymede's magnetosphere. *Geophysical Research Letters*, *43*, 4745–4754. https://doi.org/10.1002/2016GL068363

Frank, L. A., Ackerson, K. L., Lee, J. A., English, M. R., & Pickett, G. L. (1992). The plasma instrumentation for the Galileo mission. *Space Science Reviews*, *60*(1–4), 283–304. https://doi.org/10.1007/978-94-011-2512-3_11

Frank, L. A., Ackerson, K. L., Wolfe, J., & Mihalov, J. (1976). Observations of plasmas in the Jovian magnetosphere. *Journal of Geophysical Research*, *81*(4), 457–468. https://doi.org/10.1029/JA081i004p00457

Grasset, O., Dougherty, M., Coustenis, A., Bunce, E., Erd, C., Titov, D., et al. (2013). Jupiter icy moons explorer (juice): An ESA mission to orbit Ganymede and to characterise the Jupiter system. *Planetary and Space Science*, *78*, 1–21. https://doi.org/10.1016/j.pss.2012.12.002

Gurnett, D. A., Kurth, W. S., Roux, A., Bolton, S. J., & Kennel, C. F. (1996). Evidence for a magnetosphere at Ganymede from plasma-wave observations by the Galileo spacecraft. *Nature*, *384*, 535–537. https://doi.org/10.1038/384535a0

Hamrin, M., Andersson, L., Vaivads, A., Pitkänen, T., & Gunell, H. (2015). The use of the power density for identifying reconnection regions. *Journal of Geophysical Research: Space Physics*, *120*, 8644–8662. https://doi.org/10.1002/2015JA021535

Hamrin, M., Marghitu, O., Norqvist, P., Buchert, S., André, M., Klecker, B., & Dandouras, I. (2011). Energy conversion regions as observed by cluster in the plasma sheet. *Journal of Geophysical Research*, *116*, A00K08. https://doi.org/10.1029/2010JA016383

Jia, X., Kivelson, M. G., Khurana, K. K., & Walker, R. J. (2009a). Magnetic fields of the satellites of Jupiter and Saturn. *Space Science Reviews*, *152*(1–4), 271–305. https://doi.org/10.1007/978-1-4419-5901-0_9

Jia, X., Kivelson, M. G., Khurana, K. K., & Walker, R. J. (2009b). Properties of Ganymede's magnetosphere inferred from improved three-dimensional MHD simulations. *Journal of Geophysical Research*, *114*, A09209. https://doi.org/10.1029/2009JA014375

Jia, X., Walker, R. J., Kivelson, M. G., Khurana, K. K., & Linker, J. A. (2008). Three-dimensional MHD simulations of Ganymede's magnetosphere. *Journal of Geophysical Research*, *113*, A06212. https://doi.org/10.1029/2007JA012748

Jia, X., Walker, R. J., Kivelson, M. G., Khurana, K. K., & Linker, J. A. (2010). Dynamics of Ganymede's magnetopause: Intermittent reconnection under steady external conditions. *Journal of Geophysical Research*, *115*, A12202. https://doi.org/10.1029/2010JA015771

Kivelson, M. G., Bagenal, F., Kurth, W. S., Neubauer, F. M., Paranicas, C., & Saur, J. (2004). Magnetospheric interactions with satellites. In *Jupiter—The planet, satellites and magnetosphere* (Chap. 21). Cambridge University Press.

Kivelson, M. G., Khurana, K., Coroniti, F., Joy, S., Russell, C., Walker, R., et al. (1997). The magnetic field and magnetosphere of Ganymede. *Geophysical Research Letters*, *24*(17), 2155–2158. https://doi.org/10.1029/97GL02201

Kivelson, M. G., Khurana, K. K., Russell, C. T., Walker, R. J., Warnecke, J., Coroniti, F. V., et al. (1996). Discovery of Ganymede's magnetic field by the Galileo spacecraft. *Nature*, *384*, 537–541. https://doi.org/10.1038/384537a0

Kivelson, M. G., Khurana, K. K., & Volwerk, M. (2002). The permanent and inductive magnetic moments of Ganymede. *Icarus*, *157*(2), 507–522. https://doi.org/10.1006/icar.2002.6834

Kivelson, M. G., Warnecke, J., Bennett, L., Joy, S., Khurana, K., Linker, J., et al. (1998). Ganymede's magnetosphere: Magnetometer overview. *Journal of Geophysical Research*, *103*(E9), 19963–19972. https://doi.org/10.1029/98JE00227

Kopp, A., & Ip, W. (2002). Resistive MHD simulations of Ganymede's magnetosphere 1. Time variabilities of the magnetic field topology. *Journal of Geophysical Research*, *107*(A12), 1490. https://doi.org/10.1029/2001JA005071

Krimigis, S. M., Armstrong, T., Axford, W., Bostrom, C., Fan, C., Gloeckler, G., et al. (1979). Hot plasma environment at Jupiter: Voyager 2 results. *Science*, *206*(4421), 977–984. https://doi.org/10.1126/science.206.4421.977

Lindkvist, J., Hamrin, M., Gunell, H., Nilsson, H., Wedlund, C. S., Kallio, E., et al. (2018). Energy conversion in cometary atmospheres-hybrid modeling of 67p/Churyumov–Gerasimenko. *Astronomy & Astrophysics*, *616*, A81. https://doi.org/10.1051/0004-6361/201732353

Liuzzo, L., Poppe, A. R., Paranicas, C., Nénon, Q., Fatemi, S., & Simon, S. (2020). Variability in the energetic electron bombardment of Ganymede. *Journal of Geophysical Research: Space Physics*, *125*, e2020JA028347. https://doi.org/10.1029/2020JA028347

Neubauer, F. M. (1998). The sub-Alfvénic interaction of the Galilean satellites with the Jovian magnetosphere. *Journal of Geophysical Research*, *103*(E9), 19843–19866. https://doi.org/10.1029/97JE03370

Omelchenko, Y. A., & Karimabadi, H. (2006). Event-driven, hybrid particle-in-cell simulation: A new paradigm for multi-scale plasma modeling. *Journal of Computational Physics*, *216*(1), 153–178. https://doi.org/10.1016/j.jcp.2005.11.029

Paschmann, G., Øieroset, M., & Phan, T. (2013). In-situ observations of reconnection in space. *Space Science Reviews*, *178*(2–4), 385–417. https://doi.org/10.1007/s11214-012-9957-2

Paty, C., & Winglee, R. (2004). Multi-fluid simulations of Ganymede's magnetosphere. *Geophysical Research Letters*, *31*, L24806. https://doi.org/10.1029/2004GL021220

Phan, T. D., Gosling, J., Paschmann, G., Pasma, C., Drake, J., Øieroset, M., et al. (2010). The dependence of magnetic reconnection on plasma β and magnetic shear: Evidence from solar wind observations. *The Astrophysical Journal Letters*, *719*(2), L199–L203. https://doi.org/10.1088/2041-8205/719/2/l199

Plainaki, C., Massetti, S., Jia, X., Mura, A., Milillo, A., Grassi, D., et al. (2020). Kinetic simulations of the Jovian energetic ion circulation around Ganymede. *The Astrophysical Journal*, *900*(1), 74. https://doi.org/10.3847/1538-4357/aba94c

Plainaki, C., Milillo, A., Massetti, S., Mura, A., Jia, X., Orsini, S., et al. (2015). The H_2O and O_2 exospheres of Ganymede: The result of a complex interaction between the Jovian magnetospheric ions and the icy moon. *Icarus*, *245*, 306–319. https://doi.org/10.1016/j.icarus.2014.09.018

Poppe, A. R., Fatemi, S., & Khurana, K. K. (2018). Thermal and energetic ion dynamics in Ganymede's magnetosphere. *Journal of Geophysical Research: Space Physics*, *123*, 4614–4637. https://doi.org/10.1029/2018JA025312

Rosenqvist, L., Vaivads, A., Retinò, A., Phan, T., Opgenoorth, H., Dandouras, I., & Buchert, S. (2008). Modulated reconnection rate and energy conversion at the magnetopause under steady IMF conditions. *Geophysical Research Letters*, *35*, L08104. https://doi.org/10.1029/2007GL032868

Russell, C. T. (2000). The solar wind interaction with the earth's magnetosphere: A tutorial. *IEEE Transactions on Plasma Science*, *28*(6), 1818–1830. https://doi.org/10.1109/27.902211

Tóth, G., Jia, X., Markidis, S., Peng, I. B., Chen, Y., Daldorff, L. K. S., & Dorelli, J. C. (2016). Extended magnetohydrodynamics with embedded particle-in-cell simulation of Ganymede's magnetosphere. *Journal of Geophysical Research: Space Physics*, *121*, 1273–1293. https://doi.org/10.1002/2015JA021997

Vasyliūnas, V. M., & Eviatar, A. (2000). Outflow of ions from Ganymede: A reinterpretation. *Geophysical Research Letters*, *27*(9), 1347–1349. https://doi.org/10.1029/2000GL003739

Volwerk, M., Kivelson, M. G., Khurana, K. K., & McPherron, R. L. (1999). Probing Ganymede's magnetosphere with field line resonances. *Journal of Geophysical Research*, *104*(A7), 14729–14738. https://doi.org/10.1029/1999JA900161

Williams, D. J., Mauk, B., & McEntire, R. W. (1998). Properties of Ganymede's magnetosphere as revealed by energetic particle observations. *Journal of Geophysical Research*, *103*, 17523–17534. https://doi.org/10.1029/98JA01370

Williams, D. J., Mauk, B. H., McEntire, R. W., Roelof, E. C., Armstrong, T. P., Wilken, B., et al. (1997). Energetic particle signatures at Ganymede: Implications for Ganymede's magnetic field. *Geophysical Research Letters*, *24*(17), 2163–2166. https://doi.org/10.1029/97GL01931

Zhou, H., Tóth, G., Jia, X., & Chen, Y. (2020). Reconnection-driven dynamics at Ganymede's upstream magnetosphere: 3-d global Hall MHD and MHD-epic simulations. *Journal of Geophysical Research: Space Physics*, *125*, e2020JA028162. https://doi.org/10.1029/2020JA028162

Zhou, H., Tóth, G., Jia, X., Chen, Y., & Markidis, S. (2019). Embedded kinetic simulation of Ganymede's magnetosphere: Improvements and inferences. *Journal of Geophysical Research: Space Physics*, *124*, 5441–5460. https://doi.org/10.1029/2019JA026643